PERFORMANCE EVALUATION OF PHOTOVOLTAIC (PV) MODULES UNDER DIFFERENT DEPLOYMENT CONDITIONS

A THESIS SUBMITTED IN PARTIAL FULLFILMENT

OF THE REQUIREMENTS FOR THE DEGREE OF

MASTER OF SCIENCE IN PHYSICS

OF

UNIVERSITY OF NAMIBIA

BY

POLAND AMUTENYA MICHAEL

(201069075)

APRIL, 2021

MAIN SUPERVISOR:
PROF. ERNEST VAN DYK
(NELSON MANDELA UNIVERSITY)

CO-SUPERVISOR:
DR PETJA DOBREVA
(UNIVERSITY OF NAMIBIA)

Abstract

The purpose of this thesis is to evaluate the performance of solar modules, comprising various PV technologies, subject to different climatic conditions. The assessed PV technologies comprises of commercially available technologies and included Cadmium Telluride (CdTe), Copper Indium diSelenide (CIS), amorphous silicon (a-Si)and polycrystalline silicon (p-Si) modules.

Commercially available photovoltaic (PV) modules currently are comprised of two main groups: crystalline silicon modules and thin film modules. The thin film modules are cheaper due to lower production cost. They also exhibit lower temperature coefficients compared to crystalline silicon. There is a perception in the PV industry that thin film modules exhibit superior performance in hot climates and that they show better tolerance and performance in lower solar radiation locations. Our task was to determine if there is scientific evidence for such perceptions.

Measurements were done at two stations in South Africa with different climates: Port Elizabeth (PE), having a humid, relatively cool and with high cloud cover and Johannesburg (JB), having a warm, semi-arid and low cloud cover climate. In PE, one year of operation data for power output and module temperature measured at one minute time resolution were collected from the site while the GHI and ambient temperatures were measured from the site but downloaded from the SAURAN website. In JB, the power output and module temperature data measured at one minute time resolution were collected for a period of 6 months.

The assessment was based on the following performance indicators: specific yield (SY), specific yield per unit land/roof area occupied by modules (SY/A) and the relative module efficiency ($\eta_{rel.}$) for sunny (high irradiance) days and cloudy (low irradiance) days in each location. Statistical assessment of the performance indicators for each module type was performed with ANOVA test. The Tukey post-hoc test at 5% significance level was used for comparison of the daily SY, SY/A, $\eta_{rel.}$ and average module temperatures between the different technologies at each location.

A regression model was created to determine the extent of the impact of ambient conditions on the energy output of the modules. Our findings indicate that the solar radiation and ambient temperature have a strong impact on the module's SY, with the SY increasing linearly with the solar radiation while decreasing linearly with the ambient temperature during sunny days. Our findings further shows that the performance of all PV technology types are comparable in cloudy conditions at both locations. Under sunny conditions, CIS shows the highest SY in both locations, CdTe shows the highest SY/A in the warm and sunny JB climate while p-Si shows the highest SY/A under the cool and cloudy climate of PE, and a-Si shows the lowest SY, SY/A and $\eta_{rel.}$ in PE. Furthermore, CIS remained the coolest and p-Si the hottest in the JB location. In PE, all modules were equally cool on average.

In conclusion, significant difference in performance between different PV technologies is only observed during sunny conditions. In addition, the established differences during sunny conditions were not technology specific but rather dependent of the type of performance indicator assessed. Thin film technologies have shown vast differences in performance between technologies and between climatic conditions. The superior performance of thin film technologies in cloudy conditions could not be established. These results are based only on the first year of module deployment and can be expected to change with time due to module degradation.

Contents

List of Tables

List of Figures

List of Abbreviations

AM - Air Mass

ANOVA - Analysis of Variance

APE - Average Photon Energy

a-Si - Amorphous Silicon

CdTe - Cadmium Telluride

CI - Confidence Interval

CIGS - Copper Indium Gallium diSelenide

CIS - Copper Indium diSelenide

DHI - Diffuse Horizontal Irradiance

DNI - Direct Normal Irradiance

GaAs - Gallium Arsenide

GHI - Global Horizontal Irradiance

IV - Current-Voltage

JHB - Johannesburg

K-G - Köppen-Geiger

m-Si - Monocrystalline Silicon

MPP - Maximum Power Point

NMU - Nelson Mandela University

ORF - Outdoor Research Facility

PE - Port Elizabeth

POA - Plane of Array

p-Si - Polycrystalline Silicon

Q-Q - Quantile-Quantile

STC - Standard Testing Conditions

SWE - Staebler-Wronski Effect

SY - Specific Yield

SY/A - Specific Yield per Area

T_{amb} - Ambient Temperature

T_{mod} - Module Temperature

TPT - Tedlar Polyester Tedlar

VIF - Variance Inflation Factor

Acknowledgements

Firstly, I wish to express my deepest gratitude to my co-supervisor Dr. Petja Dobreva for working so closely with me. Although things were tough and I was on the edge of giving up, she pushed me to sharpen my thinking and make sure I have grasp the subject matter and not just submit for the sake of submitting. Without her persistent feedbacks and unwavering guidance, the goal of this project would not be possible.

Secondly, I would like to acknowledge my main supervisor Dr. Ernest Van Dyk for his guidance in formulating the structure of the thesis and making transport and accommodation arrangements for my visit to the Nelson Mandela University for my data collection.

I would like to show appreciation to Dr. Ross Shultz for picking me from the guesthouse to the Nelson Mandela University residence, took me for shopping and gave me an orientation on the system operation and helped me with data collection.

Further, I would like to appreciate the support given by the entire Department of Physics staff of the Nelson Mandela University during my stay while collecting data for my project.

Lastly but not least, I would like to acknowledge the HOD of the Department of Physics at the University of Namibia, Dr. Riaan Steenkamp for his continuous support in encouraging staffs of the Department to further their studies.

Dedications

This thesis is dedicated to all renewable energy enthusiast.

Declarations

I, Poland Amutenya Michael, declare hereby that this study is a true reflection of my own research, and that this work, or part thereof has not been submitted for a degree in any other institution of higher education.

No part of this thesis may be reproduced, stored in any retrieval system, or transmitted in any form, or by means (e.g. electronic, mechanical, photocopying, recording or otherwise) without the prior permission of the author, or University of Namibia in that behalf.

I, Poland Amutenya Michael, grand The University of Namibia the right to reproduce this thesis in whole or in part, in any manner or format, which The University of Namibia may deem fit, for any person or institution requiring it for study and research; providing that The University of Namibia shall waive this right if the whole thesis has been or is being published in a manner satisfactory to the University.

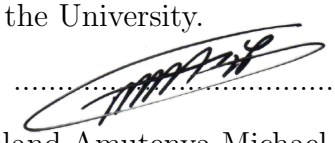

Date: 25 March 2021

Poland Amutenya Michael

Chapter 1

Introduction

1.1 Background of the study

One of the challenges faced by Namibia is the inadequacy of domestic power generation in meeting current and projected electrical energy demand [6]. Photovoltaic (PV) electricity generation is one of the promising electrical energy generation option. Since Namibia receives large amount of solar energy [7], extensive use of PV technology and systems can dramatically reduce the electricity shortage. Commercially available solar modules utilize semiconductor solar cells of different PV technologies such as monocrystalline (m-Si), polycrystalline (p-Si), amorphous silicon (a-Si), Copper Indium Gallium diSelenide (CIGS) and Cadmium Telluride (CdTe). The performance of PV modules depends on the type of PV technology and on the climatic and local environmental conditions and gradually deteriorates through the years [8].

The findings of a study done at 8 different locations in Japan by [9] indicates that the performance of p-Si modules is more influenced by module temperature than it is affected by the solar spectrum. This is a result of a larger negative temperature coefficient for power in p-Si modules than in a-Si modules. The same study reported a strong dependence of the performance of a-Si modules on solar spectrum and small dependence on the module temperature. It has been reported that it is normally difficult to evaluate the effect of module temperature

on the performance of a-Si modules in the absence of its history of operation, because the history of the module temperature needs to be taken into account as it contribute to thermal annealing which results in increased performance.

Another study in Japan by [10] showed that the outdoor performance of the p-Si modules depends mostly on the module temperature, while that of the a-Si modules mainly depends on the average photon energy (APE), which is the average energy per photon of the spectrum. A high value of APE indicates a dominance of blue light in the spectrum and low values indicates a dominance of red light in the spectrum. Since a-Si modules have a small spectral response(in the blue region only) compared to the p-Si modules(in the blue to red region), a-Si modules are more severely effected by seasonal variations in spectral distribution than p-Si modules.

Further, the performance of a-Si has been reported to increase in summer and under diffuse irradiance on cloudy days due to a bluer rich spectrum (high APE) in these conditions [11] [12].

The climatic conditions in Namibia can be quite diverse, with the desert along the coast and in the south but having an arid north central and north east areas [5]. It is therefore essential that the performance of the different types of modules is assessed under actual operating conditions so that the best suited modules are used in future applications in Namibia.

1.2 Problem statement

The energy output of PV modules is affected by the amount of solar radiation, type of PV technology, climatic and other factors. Measurements and analysis of PV technologies' performance in Namibian conditions has not been previously done. Hence a need for this research to determine suitable PV technologies for different climates in Namibia.

1.3 Objectives

(a) Measure the actual energy yield of p-Si, a-Si, CIGS and CdTe modules under various climatic conditions.

(b) Analyse the energy yield of the different PV technologies and arrive at recommendations of best suited PV technology for each climate type in Namibia.

1.4 Significance of the study

This study will have tangible outputs in the form of recommendations on optimal choice of PV technologies for the various climatic regions in Namibia.

1.5 Limitation of the study

Due to a lack of local research facilities in photovoltaics, the measurements are done at energy yield measuring stations in South Africa having different climates. The stations are located in areas with similar climatic conditions to those in Namibia based on the Kppen-Geiger climate classification [13]. The measuring stations are managed by the Outdoor research facility (ORF) at Nelson Mandela University (NMU), Port Elizabeth, South Africa.

1.6 Delimitation of the study

This study is restricted to commercially available PV technologies.

1.7 Thesis outline

Chapter 1 provides background information about the study. This includes problem statement, objectives, significance of the study, limitation of the study and delimitation of the study.

Chapter 2 introduces the components and variation in solar radiation throughout the year due to the change in solar path and atmospheric constituents. The effect of solar radiation and ambient temperature on the maximum power output of the module has also been presented. Furthermore, the differences between commercially available PV technologies has been presented. Chapter 2 concludes with outdoor performance indicators that could be used to make the right choice of best performing PV technology under the given operating climatic conditions.

Chapter 3 presents the climatic characteristics of the research sites. It includes the data measuring equipments, modules used at each research site as well as the quantities measured at each research site. Thereafter, the statistical tests used to analyze the data and the methodological approach used has been presented.

In Chapter 4, the performance of the different PV technologies at both locations is presented. The best performing technology per performance indicator at each location is also presented.

Chapter 5 presents the summary of the research, discussion of major findings, recommendations, limitations and areas of further research.

Chapter 2

Theoretical background

This chapter focuses on the review of the source, components of solar radiation and its variation during different times of the year. The components of solar radiation on a sunny and cloudy day is also presented. This is important for the understanding of the spectral distribution on these days, one of the factor responsible for the difference in performance between PV modules of different technologies. The design and model of a real solar cell will be discussed. The review on the effect of solar radiation and temperature on the output of the solar cell is also presented. Lastly, PV module performance indicators are introduced.

2.1 The solar resource and climatic conditions

The sun is the source of solar radiation on earth. The solar radiation incident on the earth's surface varies as the earth rotates around the sun in a slightly elliptical path. The amount of solar radiation incident on the surface of the earth's atmosphere perpendicularly (extraterrestrial radiation) has an average value of $1353\,\mathrm{W\,m^{-2}}$ and is referred to as the solar constant. The following points in the solar path are of importance:

- Equinox - The time/date (twice a year) at which the sun shines directly on the equator, when the day and night are of equal length (about 21 September and 21 March)

- Solstice - twice a year, the summer solstice and the winter solstice, when the sun reaches its highest or lowest point in the sky at noon, marked by the longest and shortest days (around 21 December and 21 June), respectively.

The amount of solar radiation that arrives on the earth's surface is always less than the solar constant. The reduction in solar radiation is due to the absorption, reflection or scattering of the solar radiation by the particles in the earth's atmosphere as illustrated in figure 2.1.

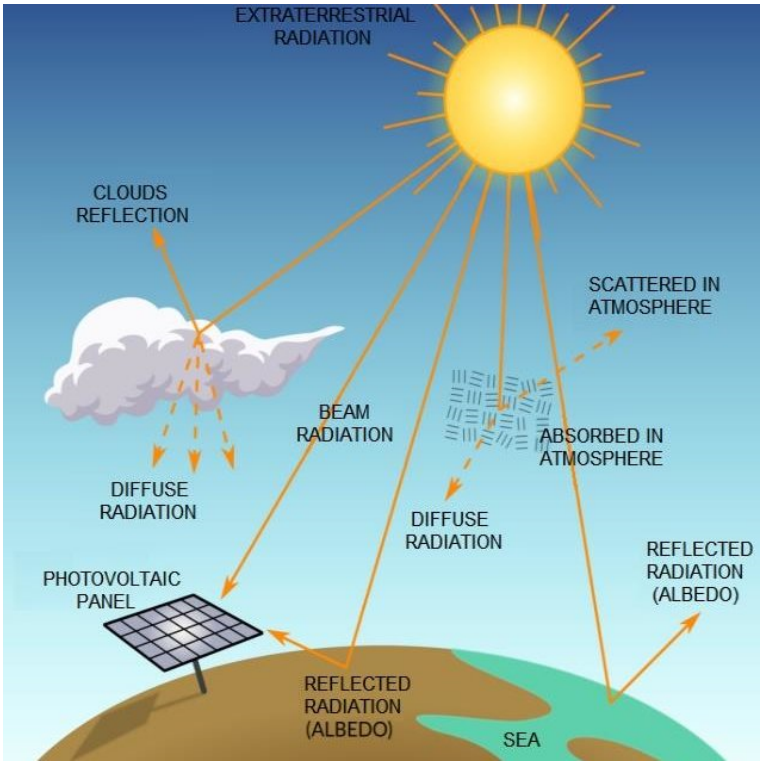

Figure 2.1: The attenuation of extraterrestrial irradiance in the earth's atmosphere [2].

The amount of solar radiation incident on an area on the earth's surface depends on the latitude of the location, the season of the year, the time of the day and the cloudiness of the sky. In short, the amount of solar radiation received at a location depends on the sun's position and the atmospheric conditions of that location.

2.1.1 Solar Spectrum

The Sun emits solar radiation of all wavelengths, but peaks in the visible wavelengths. The spectral distribution, which shows the relative weights (power density) of individual wavelengths plotted over all wavelengths is shown in figure 2.2. The figure displays the spectrum of sun rays outside the earth's atmosphere (AM0 spectrum) and the commonly used spectrum in solar applications (AM1.5 spectrum). The peak of the spectrum is within the visible spectrum, but there are still significant amounts of shorter (UV) and longer (infrared)wavelengths present.

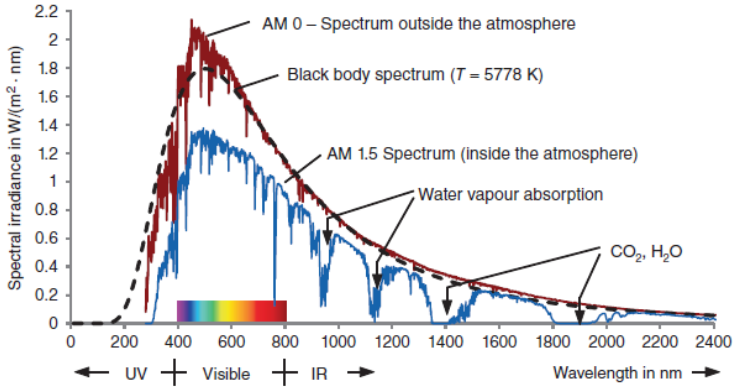

Figure 2.2: Spectral distribution inside and outside the earth's atmosphere

2.1.2 Solar radiation on a horizontal plane on the earth's surface

The amount of solar radiation incident on a horizontal surface on the earth's surface is divided into three parts: Direct Normal Irradiance (DNI), Diffuse Horizontal Irradiance (DHI) and Global Horizontal Irradiance (GHI). The irradiance is defined as the power incident on a surface per unit area, it has SI unit of Watt per square meter ($\mathrm{W\,m^{-2}}$). The GHI measures the total amount of irradiance received by a square meter of surface horizontal to the ground and is measured using a pyranometer. The GHI is related to the DHI and DNI by equation (2.1). The DHI represents the amount of irradiance incident on a horizontal surface from all directions, excluding those that comes directly from the sun. The DHI

is measured with a pyranometer that is shaded from the beam irradiance. The DNI represent the component of the irradiance that is incident on a surface perpendicularly or a surface that is always held perpendicular to the direct sun rays and is typically measured with a pyrheliometer mounted on a solar tracker to ensure that it always points directly to the sun. The DNI can also be inferred from equation (2.1) once GHI and DNI are measured.

$$GHI = DHI + DNI * cos(z) \tag{2.1}$$

where z is the zenith angle. The sun's zenith angle is the angle measured between a line that points from the site towards the centre of the sun and the vertical at the location (zenith) as shown in figure 2.3.

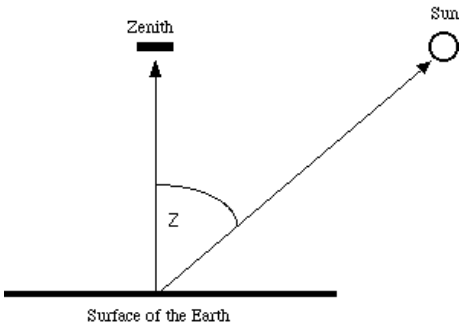

Figure 2.3: The sun's zenith angle

The irradiance incident on the plane of the module is called the plane of array (POA) irradiance. On a horizontally installed PV module (tilt angle = 0°), POA equals the GHI. The tilt angle is the angle between the horizontal line parallel to the earth surface and the plane of the module as shown in figure 2.4.

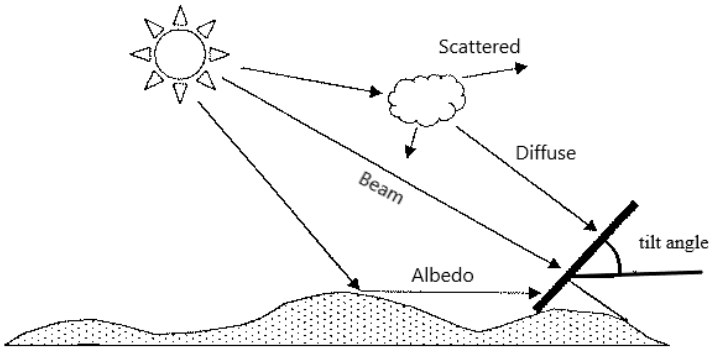

Figure 2.4: The tilt angle of a PV module

To maximize the POA irradiance, an optimum tilt angle must be chosen to ensure that the module is oriented to face the sun and will receive as much irradiance as possible during the course of the day. For a fixed module to receive maximum irradiance, the tilt angle should be approximately equal to the location's latitude [14].

2.1.3 Solar radiation on sunny and cloudy days

One of the key atmospheric constituents that largely affect the amount of solar energy incident on PV modules is cloud cover. Clouds can absorb, reflect and scatter the solar radiation, resulting in reduced direct irradiance and higher diffuse irradiance on a module and change in the spectrum of solar radiation reaching the module. PV modules of different semiconductor materials have different spectral response, therefore the change is solar spectrum due to changing atmospheric conditions, affects the performance of PV modules differently. For example, results obtained by [15] showed that the efficiencies for monocrystalline and polycrystalline modules increases with increasing air mass while that of amorphous Silicon decreases. These effects have been found to be greater under diffuse irradiance. Figure 2.5 and figure 2.6 show the components of the irradiance on a sunny and cloudy day, respectively at PE.

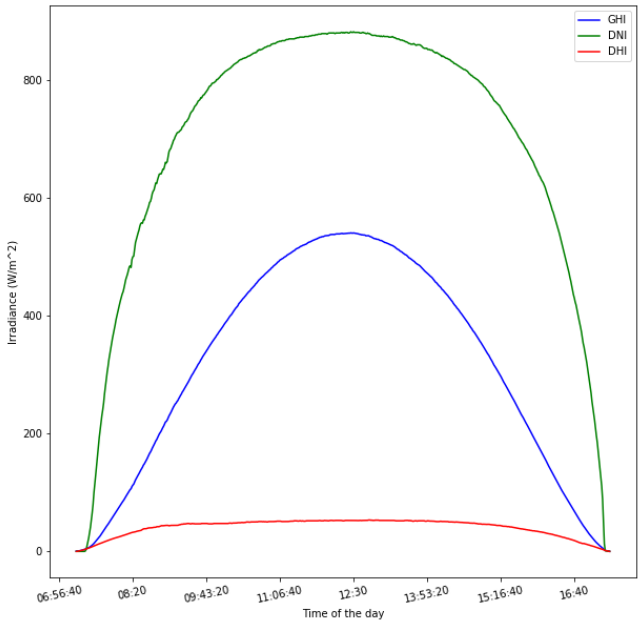

Figure 2.5: Components of the solar radiation on a sunny day as a function of time of the day on 20 June 2015 at Port Elizabeth.

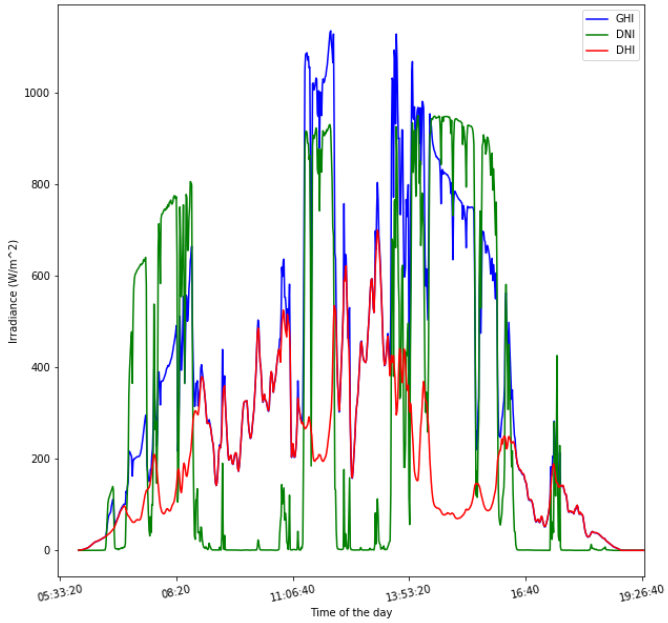

Figure 2.6: Components of the solar radiation on a cloudy day as a function of time of the day on 01 March 2015 at Port Elizabeth.

2.1.4 Köppen-Geiger climate classification

The Köppen-Geiger climate classification system is one of the most common climate classification systems in the world. The Köppen-Geiger system divides the world climate into five zones: A (tropical), B (dry), C (temperate), D (continental) and E (polar). These regions are further subdivided by seasonal precipitation and temperature. The world map of the Köppen-Geiger climate classification is shown in figure 2.7.

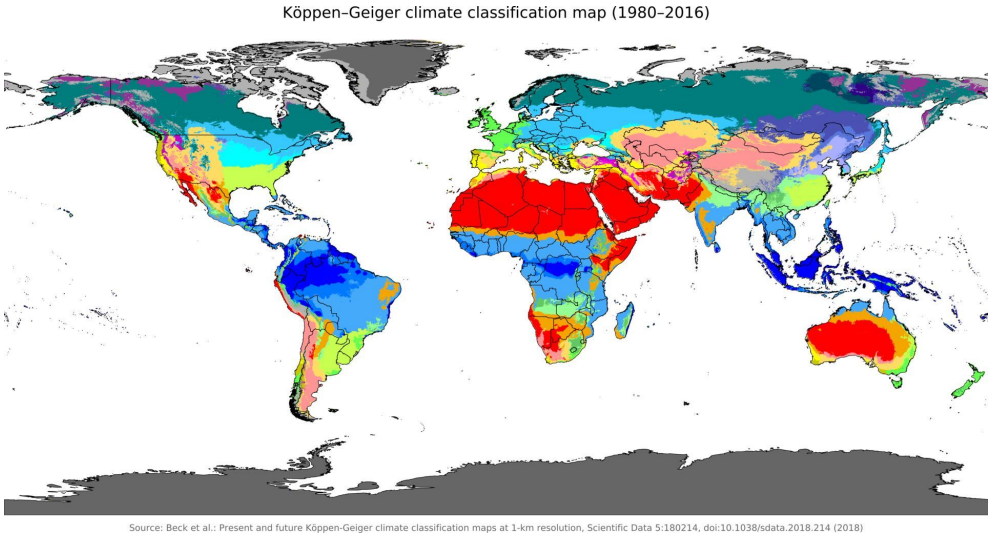

Figure 2.7: The world map of the Koppen-Geiger climate classification [3].

The performance of PV modules differs under different climatic conditions. The Köppen-Geiger climate classification can therefore be used to identify locations with similar climates and expected similar performance of PV modules.

2.2 Working principles of photovoltaic cells and modules

Solar cells are the building blocks of PV modules made from semiconductor materials. Commonly used semiconductors and their band gaps at room temperature are: Crystalline Silicon (E_g=1.12 eV), Amorphous Silicon (E_g=1.75 eV), Copper Indium diSelenide (E_g=1.02 eV) and Cadmium Telluride (E_g=1.46 eV). The

band gap (E_g) is the minimum energy required to excite an electron from its bound state in the valence band to a free state in the conduction band where it can participate in conduction [14].

The working principle of solar cells is based on the photovoltaic effect. The photovoltaic effect is the generation of a potential difference at the junction of two different materials in response to solar radiation [16].

The structure of a solar cell is shown in figure 2.8.

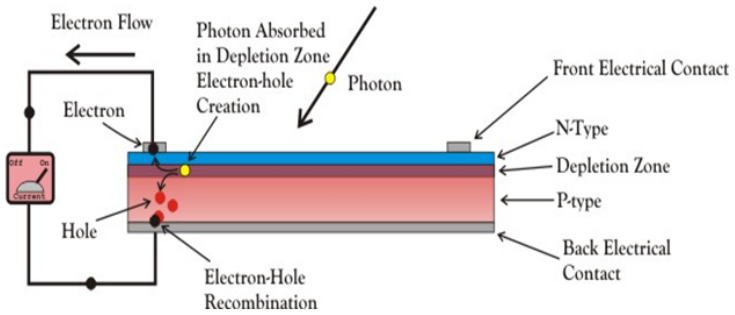

Figure 2.8: A solar cell structure [4].

A non-illuminated PV cell is a standard semiconductor diode that allows current to flow from the P-side to the N-side when forward biased. When the diode is exposed to light, the electron-hole pairs, generated by light, give rise to a photocurrent I_{Ph} that is proportional to the irradiance G and flows from the N-side to the P-side.

An ideal solar cell is modelled by a current source in parallel with a diode. In practice no solar cell is ideal. The model of a real solar cell shown in figure 2.9, contains some additional components. There exist resistance between the metal contacts and the semiconductor material and there is resistance due to the bulk of the semiconductor material. These are modelled by a single resistor(R_s) in series with the current source. Alternative current paths, that are frequently due to manufacturing defects, are modelled by a shunt resistance(R_p) in parallel with the current source. Low parallel resistance causes power losses in a PV module by providing an alternative current path for the light-generated current which decreases the current flow to the output terminals of the PV device. The effect

of parallel resistance is significant particularly at low irradiance levels, as the leakage current becomes a significant fraction of the light-generated current [14].

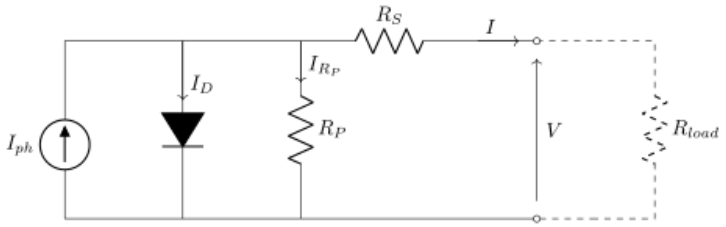

Figure 2.9: Circuit diagram of a real PV cell.

When a real PV cell is illuminated, its output current (I) is given by equation (2.2).

$$I = I_{Ph} - I_s(e^{\frac{q(V+IR_s)}{nkT}} - 1) - (\frac{V + IR_s}{R_p}) \tag{2.2}$$

where I_{Ph} - photo-generated current, V- output voltage, I_s - dark saturation current, q - elementary charge, n - Diode quality factor, $1 < n < 2$, k - Boltzmann constant, T - absolute temperature (in Kelvin)

Dark saturation current(I_s) is unwanted current flowing through the diode in the absence of incident light(hence, 'dark'), resulting from thermally excited electrons. Its value is directly proportional to the absolute temperature and inversely proportional to the material quality. The dark saturation current is an extremely important parameter which differentiates one diode from another. It is also a measure of the recombination in a device. A diode with a larger recombination will have a larger dark saturation current [14].

In a high quality PV cell the parallel resistance (R_p) is very large, therefore the last term in equation (2.2) can be neglected [17]. At open circuit, the current is zero and the open circuit voltage can be obtained from equation (2.2) and is given by equation (2.3).

$$V_{OC} = \frac{nkT}{q}\ln(1 + \frac{I_{Ph}}{I_s}) \approx \frac{nkT}{q}\ln(\frac{I_{Ph}}{I_s}) \text{ since } I_{Ph} \gg I_s \tag{2.3}$$

The open circuit voltage V_{OC} is the maximum voltage produced by an illuminated PV cell. Although V_{OC} appears to increase with increasing temperature, it actually decreases as temperature increases due to the fact that I_S increases exponentially when the temperature rises.

At short circuit, the voltage is zero and the short circuit current, (I_{SC}), can be obtained from equation (2.2) assuming R_s to be low while R_p to be very large, to obtain

$$I_{sc} \approx I_{Ph} \tag{2.4}$$

The short circuit current I_{SC} is the maximum current produced by an illuminated PV cell. The I_{SC} is proportional to the irradiance G. The effect of irradiance on V_{OC} is much weaker (only logarithmic), resulting in only a slight increase in V_{OC} with increasing irradiance. The Series resistance has no effect on V_{OC} but near the maximum power point, where relatively high current flows, the drop in potential becomes significant, resulting in reduced maximum power point.

PV cells and modules are tested and rated under a set of conditions called the Standard Testing Conditions (STC). The STC conditions are: solar irradiance of 1000W m^{-2}, Cell temperature of 25°C and Air Mass (AM) of 1.5. The standard testing conditions create a uniform testing condition which make it possible to perform comparisons of PV modules by different manufacturers.

Figure 2.10 shows the Current-Voltage (IV) curve of a typical photovoltaic module.

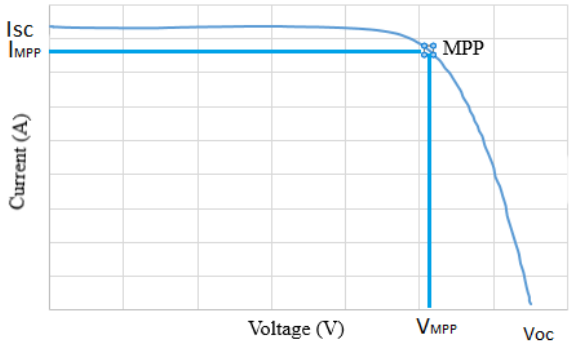

Figure 2.10: The IV curve of a generic module.

A PV module in an open or short circuit state produces no power. The maximum power output of a module referred to as the maximum power point (MPP) is given by equation (2.5)

$$P_{MPP} = V_{MPP} I_{MPP} \tag{2.5}$$

where V_{MPP} and I_{MPP} are the voltage and current at the maximum power point, respectively.

The output current and voltage of a PV module varies with irradiance and module temperature. If the irradiance is kept constant and the temperature of the module is increased, the maximum power output decreases as shown in figure 2.11.

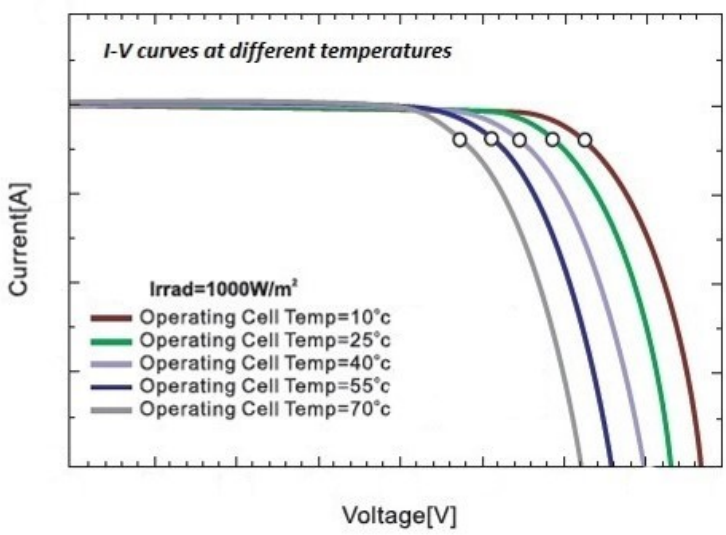

Figure 2.11: IV curves of a generic PV module under increasing module temperature.

On the other hand, if the module temperature is kept constant and the irradiance is increased, the maximum power output increases as shown in figure 2.12.

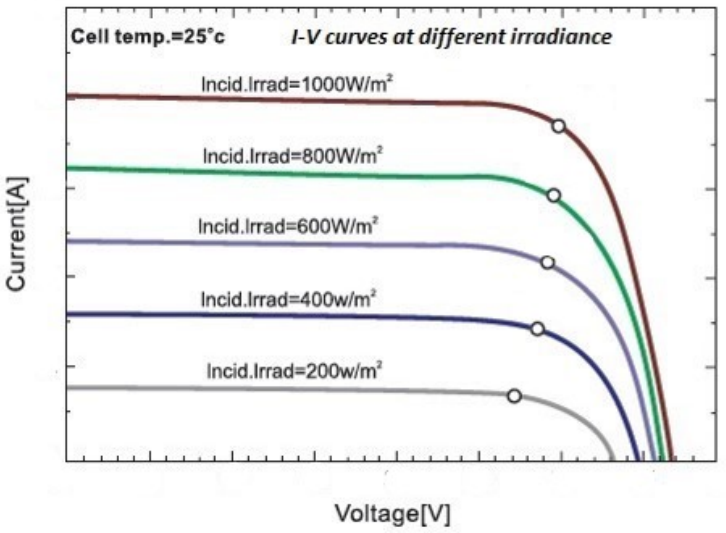

Figure 2.12: IV curves of a generic PV module under increasing irradiance.

2.2.1 Characteristics of semiconductor materials

The characteristics of the different PV modules depend on the properties of the semiconductors which themselves depend on the energy gap between the valence and conduction bands of the semiconductor. Semiconductor materials are divided into two groups: indirect and direct semiconductors.

Table 2.1 summarises the key distinctive parameters (Band gap energy(E_g), absorption mechanism and the efficiencies of the modules under Standard Testing Conditions (STC) as recorded during the year 2019 [1]) of the modules in this study. The STC conditions are: Solar irradiance of 1000W m^{-2}, Cell temperature of 25°C and Air Mass (AM) of 1.5 that determines the energy output of the PV modules.

Table 2.1: The band gap energy at 300 K and absorption mechanism for the PV technologies under investigation [1].

Technology[a]	E_g in eV	Absorption mechanism	Module STC efficiency range (%)
p-Si	1.12	Indirect	10 – 16
a-Si	1.75	Direct	3 – 7.5
CdTe	1.46	Direct	7 – 11
CIS	1.02	Direct	7.5 – 11.5

2.3 Commercial PV modules

Commercially available PV modules are categorised into two major groups: crystalline silicon and thin films. These groups are classified based on the semiconductor materials used and manufacturing procedures [18]. The crystalline silicon modules are wafer based and are of two types, monocrystalline and polycrystalline. Whereas, the thin film modules are made of thin films of semiconductor materials deposited mostly on a supporting glass substrate or superstrate. Examples are amorphous silicon (a-Si),Cadmium Telluride (CdTe),Copper Indium diSelenide (CIS), Copper Indium Gallium diSelenide (CIGS) and others [19].

2.3.1 Monocrystalline PV modules

Monocrystalline silicon PV cells are made from wafers of single crystals obtained from pure molten silicon. They exhibit predictable and uniform behaviour, are

[a]Modules data sheets in appendix.

highly efficient(module efficiency in the range of (15-18%) [17]) but are the most expensive type of modules because the manufacturing processes are slow, require highly skilled operators and are both labour and energy intensive.

2.3.2 Polycrystalline PV modules

Polycrystalline PV cells are made from molten pure silicon. During cooling it crystallizes forming irregular crystals of random sizes, shapes and orientations. Polycrystalline silicon modules have lower efficiency than monocrystalline silicon modules, with efficiency of about 11-15%. They have lower heat tolerance, therefore they perform slightly worse than monocrystalline solar panels in hot conditions. Heat can affect not only their performance but it also substantially shorten their lifespan much faster compared to the Monocrystalline modules. Polycrystalline silicon modules are much simpler to produce than the monocrystalline silicon modules, thus they cost less per module and are the most widely used silicon modules.

2.3.3 Amorphous silicon and other thin film PV modules

Amorphous silicon is the non-crystalline form of silicon. It has a random structure and due to this, not all silicon atoms are bonded to other four silicon atoms (as in crystalline silicon). The unbounded electrons therefore form dangling bonds that result in defect states in the band gap enhancing recombination. Therefore, the dangling bonds are normally saturated with hydrogen atoms to reduce the number of defect states in the band gap. The efficiency of amorphous modules is around 6-8%.

Thin-films can be deposited onto different substrate. The different types of thin-film solar cells can be categorized by the photovoltaic material that is deposited onto the substrate and other thin film modules include Cadmium telluride (CdTe), Copper indium gallium selenide (CIS/CIGS) and Gallium arsenide (GaAs). The manufacturing process is simpler, easier and cheaper than in the

crystalline cells. Another manufacturing advantage is that PV films can be easily deposited on a wide variety of both rigid and flexible substrates including glass, steel and plastics. Amorphous silicon is a direct band gap semiconductor and therefore a better light absorber than crystalline silicon.

The disadvantages of Amorphous PV modules is that, they have the lowest efficiency, requires a very large area to produce enough energy and they also degrade faster than mono- and polycrystalline PV modules. Amorphous silicon modules show significant light-induced degradation effect, in which their efficiencies degrade by about 10 - 30% when initially deployed outdoors [20]. The degradation is due to the process called the Staebler-Wronski effect(SWE). In the SWE process, the incident light breaks the weak silicon-to-silicon bonds and leaves the dangling bonds in the material, which act as recombination centers or defects. This effect however stabilizes after hundreds of hours of outdoor exposure to solar radiation. Stabilization can also be achieved by heating the module at high temperatures above 170°C [21], in a process called annealing, which reverses the degradation. After exposure to light, the degradation occurs again, but at a lower rate.

Some thin film modules experience a positive light soaking effect after illumination, which leads to an increase in their power output. For example, CIS modules generate extra energy as soon as they are exposed to outdoor solar radiation. The light soaking effect stabilizes after about 50 hours of exposure to sunlight and remains stable for the entire life cycle of the module [22].

2.4 PV module outdoor performance indicators

The choice of modules for application at a specific location should be carefully done in such a way that maximum possible output is attained under the specific climatic conditions. The amount of energy produced by the modules at a specific location strongly depends on the solar radiation and ambient temperature of that location. The energy output also depends on the characteristics of the

modules, which include temperature coefficients and efficiencies. The following performance indicators enable us to compare the performance of modules with different characteristics.

2.4.1 Relative efficiency ($\eta_{rel.}$)

The relative efficiency represents a fraction of the STC efficiency and is given equation (2.6).

$$\eta_{rel.} = \frac{\text{Efficiency under operating conditions}}{\text{Efficiency at STC}} \tag{2.6}$$

The relative efficiency indicates the quality of the module. Thus modules with less defects will produce higher relative efficiencies. The relative efficiency is independent of the irradiance and module areas and is suitable for comparison of modules with different rated efficiencies.

2.4.2 Specific yield (SY)

The specific yield is the hours that a module has to operate at its maximum rated power to output the energy it produced in a certain period of time. In other words, it represents the amount of energy produced per one watt of installed power of that module given by equation (2.7).

$$SY = \frac{\text{Energy output}[\text{kW h}]}{\text{Installed peak power}[\text{kW}_\text{p}]} \tag{2.7}$$

It can be seen from equation (2.7) that the specific yield does not depend on the nominal power of the module and it is therefore suitable for comparison of the performance of modules with different rated power. Thus, a module with a higher specific yield is favourable when there is plenty of space.

2.4.3 Specific yield per area (SY/A)

The specific yield per area signifies the amount of energy produced per land or roof area occupied by 1kW of a given PV technology. The SY/A is given by

equation (2.8).

$$SY/A = \frac{\text{Energy output[kW h]}}{\text{Installed power[kW}_\text{p}\text{]} \times \text{Area[m}^2\text{]}} \tag{2.8}$$

The SY/A does not depend on the nominal power or area of the module. This makes it a suitable performance indicator for modules of different nominal power and size. The type of module that generates the highest energy from the smallest area (higher SY/A) will be the preferred candidate in locations where the roof or land area is limited.

2.5 Chapter Summary

In this chapter, the variation in solar radiation during sunny and cloudy days has been presented. The components of the solar radiation has also been presented in terms of time graph vs irradiance. The variation in spectral distribution was also presented. The solar radiation and its components varies throughout the year due the change in the path of the earth as it rotates about the sun and also due to the change in atmospheric constituents throughout the year. The structure and model of a real solar cell has been presented, detailing how the amount of solar radiation and module temperatures affect the maximum power produced by the module.

The properties and differences between commercially available PV modules have been presented, leading to the outdoor performance indicators that could be used to make the right choice of the commercially available PV modules based on the climatic conditions under which the modules will operate. The presented performance indicators are: relative efficiency ($\eta_{\text{rel.}}$), specific yield (SY) and specific yield per area (SY/A).

Chapter 3

Experimental equipment and Methodology

This chapter gives an overview of the research locations, the equipment used for measurement and data collection as well as the data cleaning and preparation prior to the analysis. The analysis approach, based on the statistical tests for the performance of the available PV technologies, is also outlined in this chapter.

3.1 Research Locations

Two locations in South Africa with different climatic conditions were considered. Port Elizabeth (PE), with station coordinates: Latitude: 34.00859° S, Longitude: 25.66526°E and Elevation: 35 m above mean sea level (AMSL). Johannesburg (JHB), with location coordinates: Latitude: 26.2041°S, Longitude: 28.0473° E. Namibia lacks research facilities in photovoltaics, therefore, these locations were chosen based on similarities in climatic conditions to Namibian conditions based on the Köppen-Geiger climate classification [5]. The research locations are indicated in figure 3.1. According to the Köppen-Geiger (K-G) climate classification, PE has a warm semi-arid climate while JHB has a humid subtropical climate.

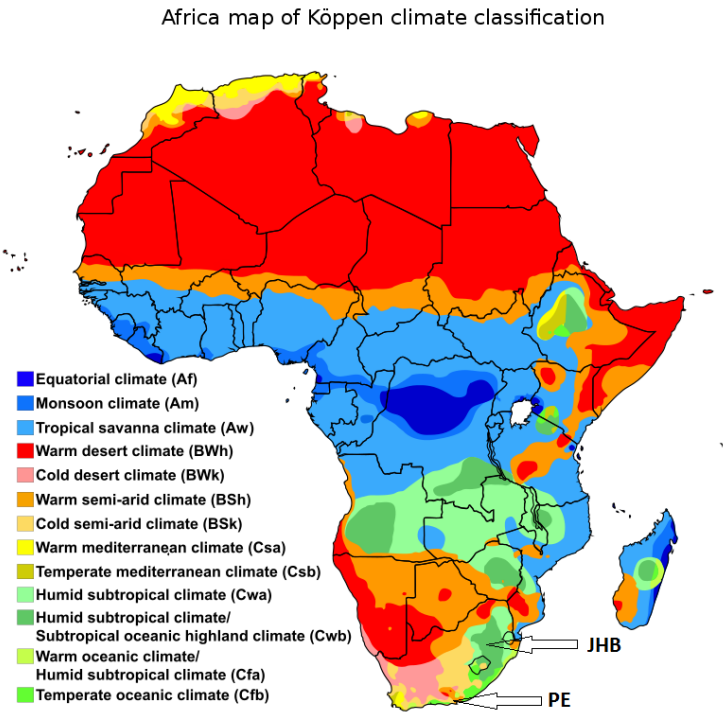

Figure 3.1: Adapted from the Köppen-Geiger climate classification map [5].

3.2 Research equipment and data collection

The following equipment and software were used in the measurement of the climatic and module parameters:

- Kipp & Zonen CMP11 unshaded Pyranometer for recording the Global Horizontal Irradiance (GHI).
- Campbell Scientific CS215 sensor for measuring the ambient temperature (T_{amb}).
- ISET sensor for measuring the plane of array (POA) irradiance.
- Sol. Connect Sensor T PT 1000 B (operating temperature range from -30°C to +105°C) attached to the back of the module for measuring the module temperature (T_{mod}).
- Papendorf Software Engineering GmbH monitoring system for importing and storing the data.

The readings of the T_{mod}, T_{amb}, POA irradiance and GHI are stored by the Papendorf Software Engineering GmbH monitoring system at a 1 minute time interval. These data can be imported as csv files for further analysis. This study was limited to commercially available PV modules. The list of modules at each location, the rated power,rated efficiency and maximum power point temperature coefficient, as well as the modules orientation is given in table 3.1.

Table 3.1: Main characteristics of modules installed at each research location

Location	PV technology	Tilt angle (°)	Rated power (W)	Rated efficiency (%)	P_{mpp} Temp. coefficient(%/°C)
Port Elizabeth	p-Si	33	240	14.7	- 0.40
	CIS	33	155	12.6	- 0.31
	a-Si	33	100	6.4	- 0.20
Johannesburg	p-Si	26	250	14.7	- 0.40
	CIS	26	155	12.6	- 0.31
	CdTe	26	110	15.3	- 0.28

All modules were installed on racks with temperature sensors attached to the back of the modules near the centre of each module. The rack installation allows free air circulation which aids the cooling of modules. In PE, all modules face North (azimuth = 0 °N) and have tilt of 33 °, which corresponds to the latitude of the location. In JHB, all the modules face North (azimuth = 0 °N) and have a tilt of 26°which also corresponds to the latitude of the location.

At the PE research site, the following data were measured at 1 minute time intervals for a period of 1 year:

- Module power output (P_{mod})
- Module temperature (T_{mod})
- POA irradiance
- GHI
- T_{amb}

At the JHB research site, the following data were also measured at 1 minute time intervals for a period of 7 months:

- P_{mod}
- T_{mod}
- POA irradiance

3.3 Statistical Analysis

The power of statistical analysis is the ability to draw conclusions about a population based on the information from the sample data [23]. To be able to accurately interpret the data depends on how we process the data and on the use of the right statistical techniques and tests to uncover patterns and trends. A few techniques used in this project are outlined below:

3.3.1 Box and whisker plot

The entire data set can be visualised with a histogram or with a box-and-whisker plot, simply referred to as a box plot. The shape of a histogram can be misleading because it depends on the choice of bins. The choice of bins is arbitrary as there is no fixed rule for partitioning the data into bins. A box plot, is free from the shortcomings of a histogram, because it summarises key statistics of the data and display them in a format that offers a quick way of examining the variation present in the data sets, at a glance. A wider range box plot indicates more variability within the data. A perfectly symmetric rectangle indicates a normally distributed data set while an asymmetric rectangle indicates a skewed data.

A box plot is useful when comparing several data sets against each other. The length of the rectangle,referred to as the interquartile range, represents 50% of the data around the median. The horizontal line through the rectangle represents the median of the data set while the lower and upper part of the rectangle represent 25% of the data below and above the median, respectively. The lower whisker marks the minimum value of the data set that is within 1.5 times the interquartile range while the upper whisker indicates the maximum value within

1.5 times the interquartile range. A perfectly symmetric rectangle indicates a normally distributed data set while an asymmetric rectangle indicates a skewed data. Figure 3.2 shows an example of the same data presented on a box plot and on a histogram with 6 bins.

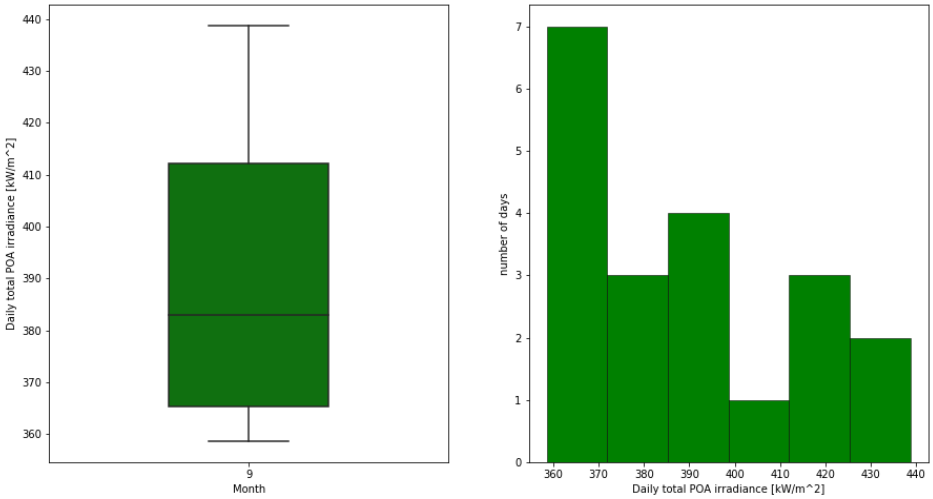

Figure 3.2: Same data shown on a box plot (Left) and on a histogram(Right).

.

It can be seen from both, the box plot and histogram, that the presented data is right skewed. However, the median, interquartile range can be determined from the box plot and not on the histogram.

3.3.2 Analysis of variance (ANOVA) and Tukey's test

Analysis of variance (ANOVA) is an inferential statistical test that compares the means of more than two data sets, accounting for the variance in each set. Assumptions underlying ANOVA include normally distributed data, similar group variances, and independence of the data groups. However, normality and variance assumptions can often be violated when dealing with smaller and unequal sample. It is therefore recommended to use sufficiently large and equal sized samples [24].

ANOVA tests the null hypothesis that all group means are equal. If an ANOVA test does not yield statistically significant difference, the Null hypothesis

is accepted, otherwise the Null hypothesis is rejected. When the null hypothesis is rejected, it can be concluded that at least one population mean is different from at least one other mean. The significance level is the probability of making a wrong decision. This means, rejecting the null hypothesis when the null hypothesis is true. The p-value of the test is the probability of finding a difference by chance. This implies that if the probability of finding by chance is small, the difference actually exist, els eif it is large, the difference does not exist. If the p-value from the ANOVA test is less than the significance level ($\alpha = 0.05$), we can reject the null hypothesis and conclude that we have sufficient evidence that at least one of the means of the groups is different from the others.

When statistical significant difference is obtained in an ANOVA, additional statistical tests are necessary to determine which of the group means differ from which other group means. The follow up tests are referred to as the post hoc tests. One of the frequently used post-hoc test is the Tukey's honest significant difference test(Tukey's HSD test).

Tukey's HSD assesses the difference between two group means by comparing the variance within a group to the variance between groups. If the variance between groups is much larger than the variance within a group then the group means are unlikely to be equal. However, if the variance within a group is about the as the variance between the groups, then the group means are likely to be equal.

In many circumstances, different post-hoc tests may lead to the same conclusions, the choice therefore normally depends on the preference of the researcher. However, for unequal sample sizes, the Tukey's HSD test is recommended.

3.3.3 Regression analysis

The goal of a regression analysis is to express the dependent(response) variable as a function of the independent (predictor) variables. To develop a regression model, one has to scatter plot the response vs predictors to determine if there are

any trends. If there appears to be a linear trend, then the Pearson's correlation coefficient can be determined to indicate the degree of linear correlation between the response and the predictors. The correlation between the predictors also need to be determined to avoid multicollinearity in the model. Multicollinearity means a high degree of correlation between two explanatory variables that including both does not explain any more the variation in the response; therefore, it suffices to include only one of the explanatory variables; including both will result in inaccurate regression coefficients. The Variance inflation factor (VIF) is an indication of the increase in inaccuracy of the regression coefficients (and increase in model error) when correlated explanatory variables are included in the model. Accepted VIF's should be less than 5. A VIF value larger than 10 is an indicator of multicollinearity [25].

Once the correlation has been determined, one can proceed to build the regression model choosing a functional relationship that best reflects causality or that best fits the available data. The regression model can be used to predict values of the response variable, to identify variables that most affect the response, or to verify hypothesized causal models of the response. A multiple linear regression model has a form defined by equation (3.1) [26].

$$Y = \beta_0 + \beta_i X_i + ... + \beta_n X_n + \varepsilon \tag{3.1}$$

where Y- dependant variable (response), β_i -regression coefficients, X_i-independent variables(explanatory variables, predictors), $i = 1$ to n- number of independent variables and ε- model error vector.

3.3.4 Analysis of regression residuals

The residual is defined as the difference between the observed value of the dependent variable and the fitted value. The most important assumption of a linear regression model is that the residuals must be completely random, unpredictable and normally distributed. The validity of the regression equation can be tested

with the residuals vs. fitted values graph, where the residuals are plotted on the y-axis and values of the response variable obtained from the regression model are plotted on the x-axis. The sum of the residuals must always be equal to zero. A correct, well specified regression model should yield randomly distributed residuals around a horizontal line drawn though zero on a residuals vs fitted values plot. If the plots display a noticeable pattern, then the regression equation is not correctly specified and the regression coefficients cannot be trusted.

3.4 Analysis approach

The data analysis was done in the Python programming language using the Pandas software library. The data was cleaned in the following sequence: cleaning out night hours data and retaining the data for which the power output of at least one module is non-zero; this is because different PV technologies have different spectral response and therefore start producing at different times in the morning. Further, filtering out cases where the POA irradiance is zero and cleaning out all missing values to avoid possible division by zero when computing performance indicators.

The data was divided into seasons (Spring, Summer, Autumn and Winter) to take into account the variation in the amount of daily solar radiation due to time of the year. To take into account the effect of cloud cover on the solar radiation incident on the modules, each season was divided into sunny and cloudy days. A day of a given season was classified as sunny if its total daily GHI is equal to or greater than 75 % of the Maximum daily GHI in that season. Otherwise it is classified as cloudy.

The mean values of the Relative efficiency ($\eta_{rel.}$), Specific Yield (SY) and specific yield per area (SY/A) for the different technologies were assessed with the Analysis of Variance (ANOVA) statistical test. The data was tested prior to the application of the ANOVA test to ensure that the assumptions of the test are met. The normality of the data was tested with the Shapiro - Wilk test

while the Levene's test was used to test for the equality of variances between the groups [27]. Even though the data would show some deviation from the normal distribution, the ANOVA test can still be used as it is fairly robust with respect to moderate deviations from normality [23].

If we fail to reject the null hypothesis, as introduced in section 3.3.2, then we know with a 95 % confidence, that the groups mean are statistically equal. However, if we reject the null hypothesis then we must run a post-hoc test to determine which group means are statistically different from each other. In this case, a Tukey post-hoc test was used.

The relationship between the SY and the ambient conditions at PE was assessed with scatter plots of SY vs GHI and SY vs T_{amb}. The strength of the relationship was determined by evaluating the Pearson's correlation coefficient between the SY & GHI and between the SY & T_{amb}.

To determine the functional dependence of the SY on the ambient conditions like GHI and T_{amb}, a multiple linear regression was performed. In this analysis the GHI and T_{amb} were found to be correlated, however, both produced statistically significant regression coefficients in the model. The variance inflation factors (VIFs) were computed to indicate the level of multicollinearity between the GHI and the T_{amb} and were found to be within the acceptable limits (VIF<5) [25].

The suitability of the selected regression model was tested by assessing the residuals of the model. If the residuals vs predicted values graph shows no pattern, i.e. the residuals appear random, then this is an indication that the functional form of the regression model is correct. In addition, the residuals of a well specified model will follow a normal probability distribution.

3.5 Chapter summary

This chapter presented the research locations with their climatic characteristics according to the K-G climate classification. It outlined the measuring and data collection equipment as well as the solar modules, used at each location in this

study. The chapter presented the quantities measured at each location: module power output, P_{mod}, module temperature, T_{mod}, ambient temperature, T_{amb}, Global horizontal irradiance, GHI and plane of array (POA) irradiance at PE and P_{mod}, T_{mod} and POA irradiance at JHB.

The statistical techniques used to analyze the data were presented. This include box plots to display the distribution of the data, Anova test to test if there is a difference between any of the means of the modules' performance indicators, Tukey's HSD test to identify between which groups the difference exist, should the Anova test find a difference in means and regression analysis to determine the dependence of the modules output on the solar radiation and ambient temperature. Lastly, a thorough methodology has been presented.

Chapter 4

Results and Discussion

In this chapter, the results and analysis of the performance of three different PV technologies at the two energy yield measuring stations in Port Elizabeth and Johannesburg are presented. The results include comparisons of module temperatures, relative efficiencies, Specific yields and Specific yield per Area. The results of a linear regression, assessing the effects of ambient conditions on the specific yield at the outdoor research facility (ORF), Port Elizabeth (PE), South Africa are also presented.

4.1 Assessment at the ORF, Port Elizabeth(PE)

4.1.1 Local climate - Solar radiation and ambient temperature at PE

Ambient conditions such as solar radiation, ambient temperature and humidity have a significant effect on the performance of PV modules [28–30]. Module performance at a given location and the variability in performance throughout the year is a function of the climatic conditions at the location. The climatic conditions analysis for PE is based on the available one year of data (starting from 01 March 2015 until 29 February 2016) for GHI and T_{amb} obtained from the weather station at this site, which have been measured at a one minute time

resolution. The variation in GHI throughout the year at the Port Elizabeth research site is illustrated by the box and whisker plot in figure 4.1 for each month of the year.

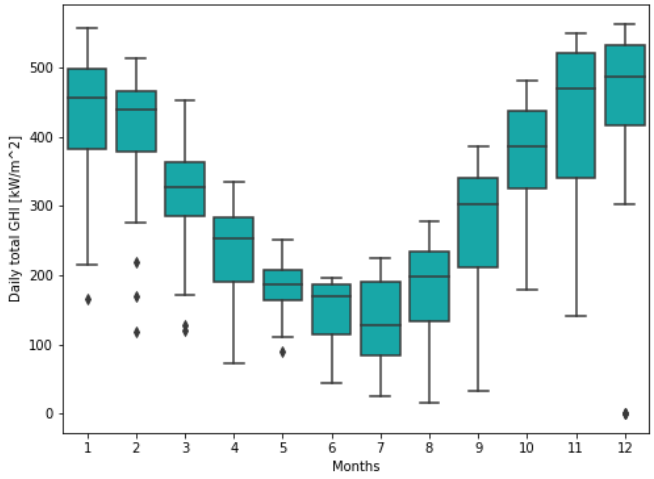

Figure 4.1: The daily total GHI for each month of the year in PE

It can be observed from figure 4.1 that the spring and summer months (September to February) are characterised by high irradiance values and a greater variability in GHI compared to the winter and autumn months (March to August) that are characterised by lower irradiance values and small variation in GHI. Greater variation in irradiance within a short period of time is an indication of frequent presence of atmospheric constituents such as clouds. Greater variability in the solar radiation will lead to greater variability in module performance. It can be expected that the modules will show a broad range in their energy output during the spring and summer month but a relatively narrow range of energy output in the winter.

The variation in average daily ambient temperature for the period from 01 March 2015 until 29 February 2016 is shown in figure 4.2.

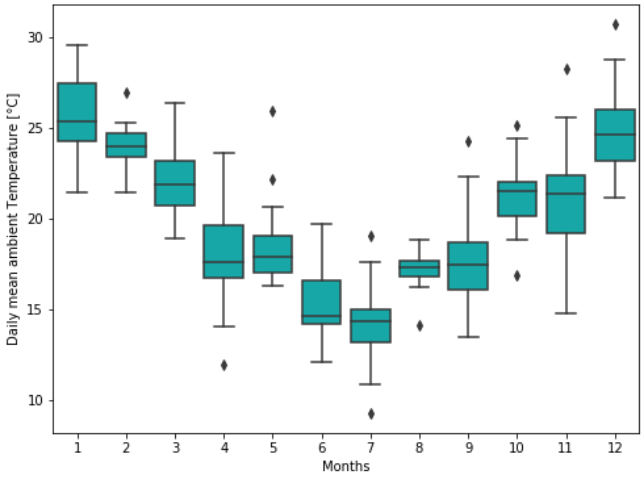

Figure 4.2: The daily mean ambient temperature for each month in PE

The average daily temperature for the daylight hours varies from about 12°C in winter to about 29 °C in summer without extreme temperature variations in a day. Large daily temperature variations lead to cell connector breakage and cracks-a dominant factor in module degradation [**?**].

Based on the criteria for sunny days defined in section 3.4, the sunny days refers to the high irradiance spring and summer days having daily total irradiance equal to or larger than 352.77 $\mathrm{kW\,m^{-2}}$. The variation in daily GHI and mean ambient temperature for the sunny days is shown in figure 4.3, which illustrates a relatively small variation in daily ambient temperature.

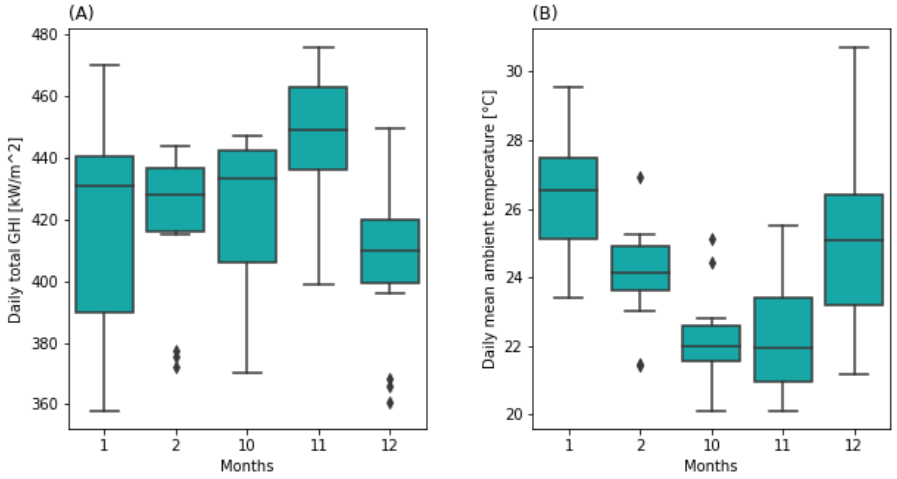

Figure 4.3: Daily total GHI (A) and mean ambient temperature (B) for the sunny days in PE

Theoretically, the ambient temperature is proportional to the solar radiation. However, from figure 4.3, the daily solar radiation is relatively high in the months of October and November but the ambient temperature is lower than the daily ambient temperature for months with comparable irradiance. The lower ambient temperature might be a result of the presence of high speed winds in those months. High speed winds aid in the cooling of modules. The wind speed data was however not available.

The cloudy days data set comprises of cloudy days from all the seasons under the criteria defined in section 3.4. All the cloudy days have a daily total GHI less than 350 kW m^{-2}. Figure 4.4 shows the variation in daily total GHI and ambient temperature for the cloudy days.

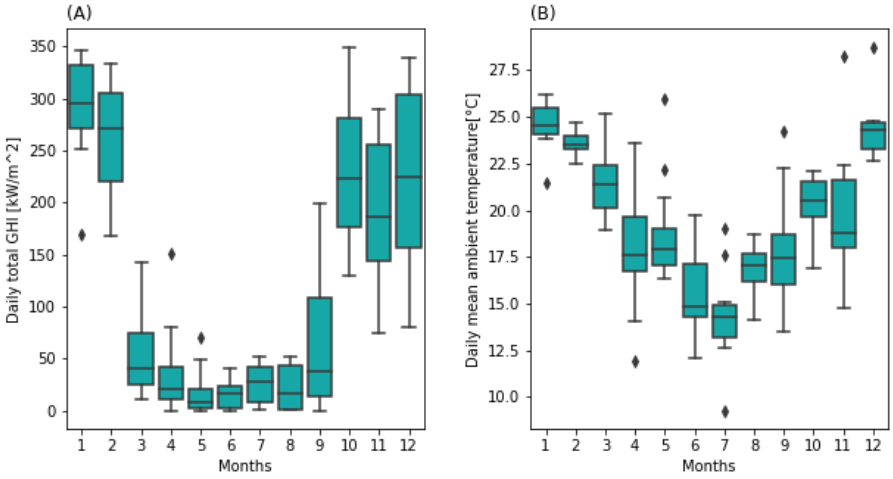

Figure 4.4: Daily, total GHI (A) and mean ambient temperatures (B) per month for the cloudy days in PE

During the assessment period, the coastal climate of PE has been characterised by nealy 67% of the days falling in the cloudy category, with the daily mean ambient temperature averaging about 20°C and the daily total GHI averaging about 200kW m^{-2}

4.1.2 Modules temperature at PE

Temperature is one of the key factor that affects the power output of the PV modules. The 17th of December 2015 was selected to serve as an example for a sunny day and in the follow up sections, whenever a single sunny day is referred, it refers to this day. The hourly values of GHI, POA and T_{amb} for this day are presented in Table table 4.1 to provide a sense of the numerical values of the solar radiation and the ambient temperature for the day.

Figure 4.5 presents the variation in module temperature and POA on the sunny day of 17 December 2015.

Table 4.1: Hourly mean data for the sunny day of 17 December 2015

```
In [1137]: 1 singlesunnyday.groupby(singlesunnyday.index.hour).mean()
```

Out[1137]:

	GHI_CMP11 W/m^2 Avg	IrrPoA_Avg[W/m^2]	Air_Temp Deg C Avg
4	3.294000	0.328500	12.615000
5	52.539667	21.800550	13.224000
6	249.043333	115.551667	18.111000
7	466.060000	317.241667	21.866000
8	685.391667	561.641667	23.037167
9	872.948333	785.083333	23.996333
10	1010.783333	951.050000	25.009167
11	1091.416667	1046.983333	26.673833
12	1105.450000	1068.666667	27.022833
13	1052.466667	1015.333333	26.277333
14	940.116667	890.066667	26.292000
15	775.715000	700.256667	26.256167
16	574.590000	455.450000	26.015000
17	343.390000	183.832833	25.397000
18	119.877167	59.709500	23.967000
19	14.080759	9.428241	22.791724

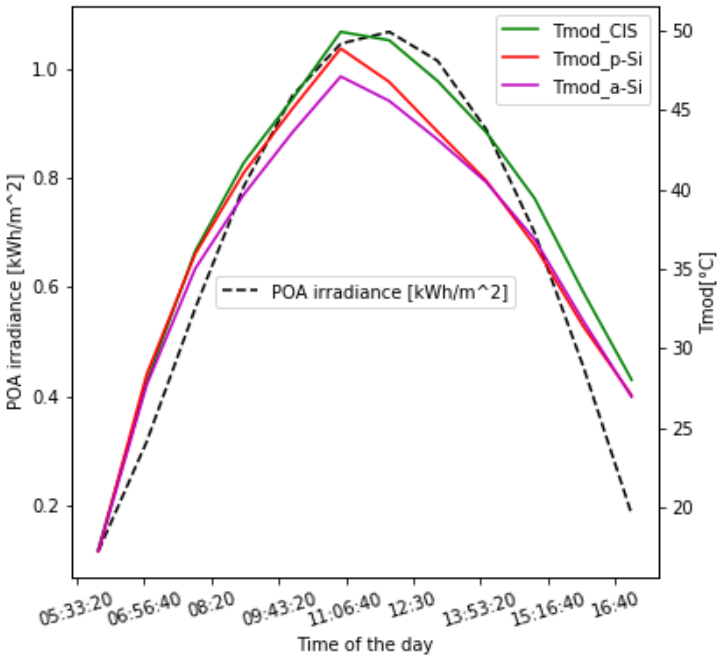

Figure 4.5: POA and T_{mod} as a function of the time of the day in PE on the sunny day of 17 December 2015

The increase and decrease in module temperature correlates well with the increase and decrease in POA as shown in figure 4.5. It is observed from figure 4.5 that CIS attained the highest temperature on the sunny day of 17 December 2015. This could be due to the fact that CIS is a glass-on-glass type of module, having a lower heat exchange capabilities compared to modules with glass on top and tedlar polyester tedlar (TPT) at the back. In addition, its dark appearance is an indication it absorbs most of the incident solar radiation. However, the lower efficiency of the CIS modules means that only a smaller portion of the absorbed solar radiation is converted to electrical energy, the rest is converted to heat. The ambient and modules temperature both depend on the solar radiation. Figure 4.6 shows the ambient and modules temperature on the sunny day of 17 December 2015.

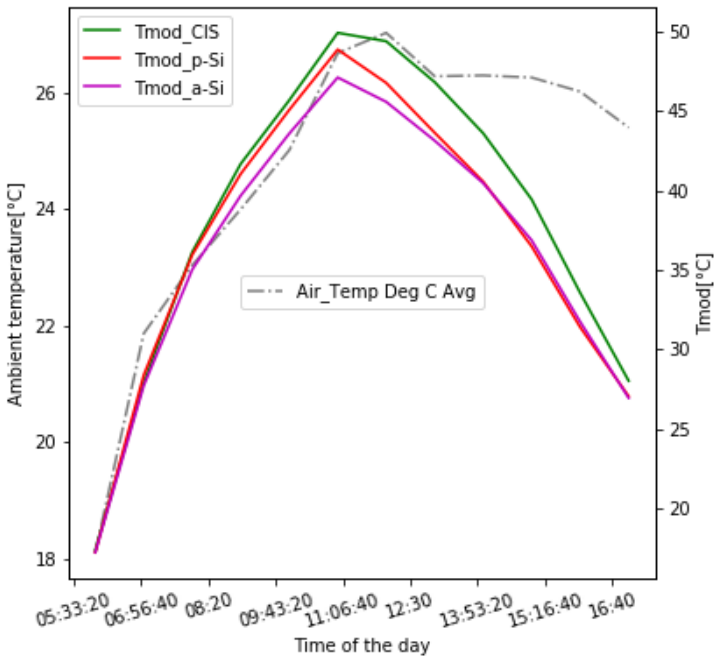

Figure 4.6: The variation in ambient and modules temperature as a function of time of the day for the sunny day of 17 December 2015

Starting from morning hours as observed from figure 4.6, the increase in ambient temperature results in an increase in module temperatures, from noon, the ambient temperature remains relatively constant while the module's temper-

atures decreases significantly. The decrease in modules' temperature is a result of the sun moving towards the horizon, resulting in less energy incident on the modules. Figure 4.6 provides an indication that a module's temperature depends far more on the POA and much less on the T_{amb}.

The mean daily module temperatures and their standard deviation on all sunny days were found to be 38.9± 5.2°C for CIS, 38.1± 4.4°C for p-Si and 37.8± 4.4°C for a-Si. Figure 4.7 shows the distribution of the modules temperature during all the sunny days. The better the vertical alignment of the boxes on the box plot, the higher the chances of not having a significant difference between the group means. On cloudy days, the distribution in daily modules temperature is shown in figure 4.8.

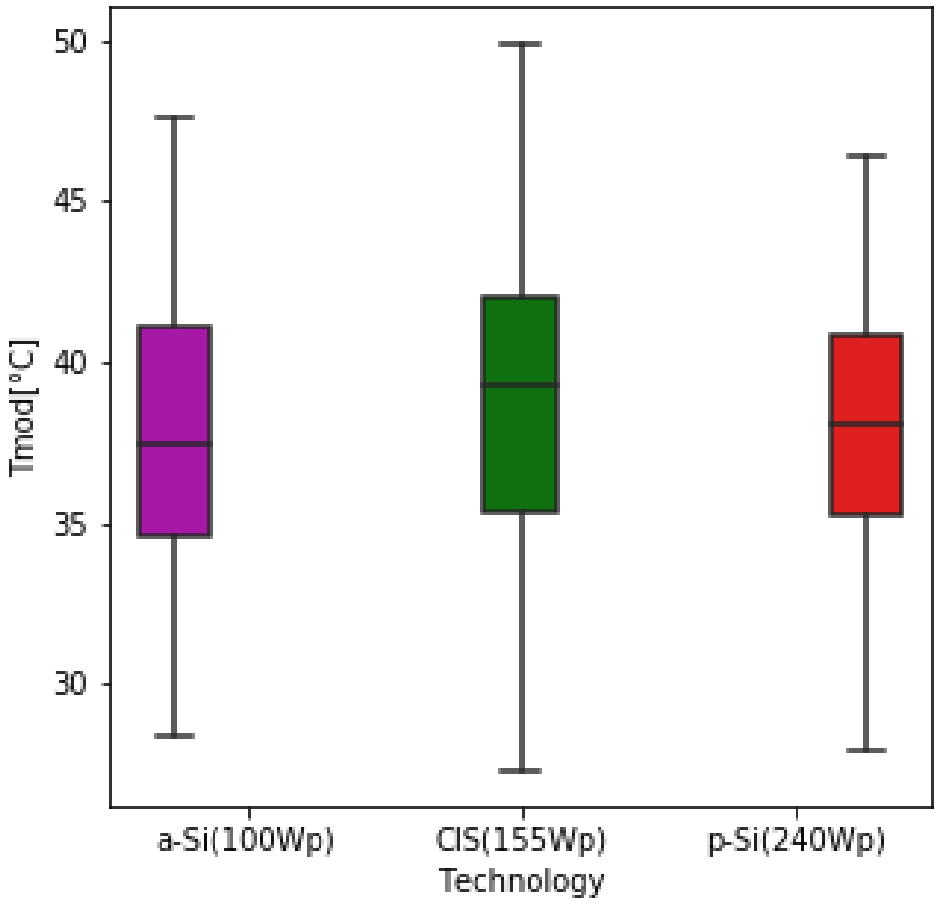

Figure 4.7: Daily mean module temperature variation for all the sunny days in PE.

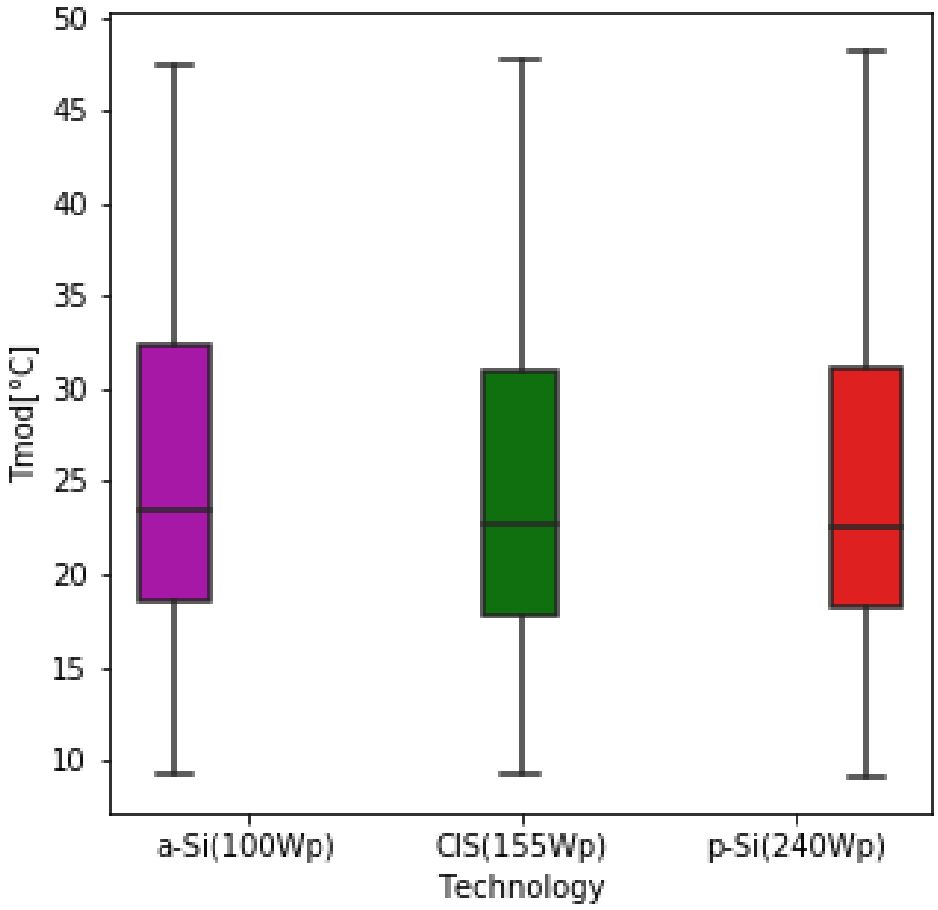

Figure 4.8: Daily mean module temperature variation for all the cloudy days in PE.

The ANOVA test on modules temperature, showed that on average, the daily modules temperature are not statistically different from one another at the 5% significance level ($p<0.05$) on both sunny and cloudy days. So that on average, on any day, no module type is significantly hotter or cooler than the others at PE location.

4.1.3 Relative Efficiency ($\eta_{rel.}$) in PE

The relative efficiency is a performance indicator as defined by equation equation (2.6). Figure 4.9 shows the variation in ambient temperature and relative efficiencies of the three modules as observed on a sunny day of 17 December 2015.

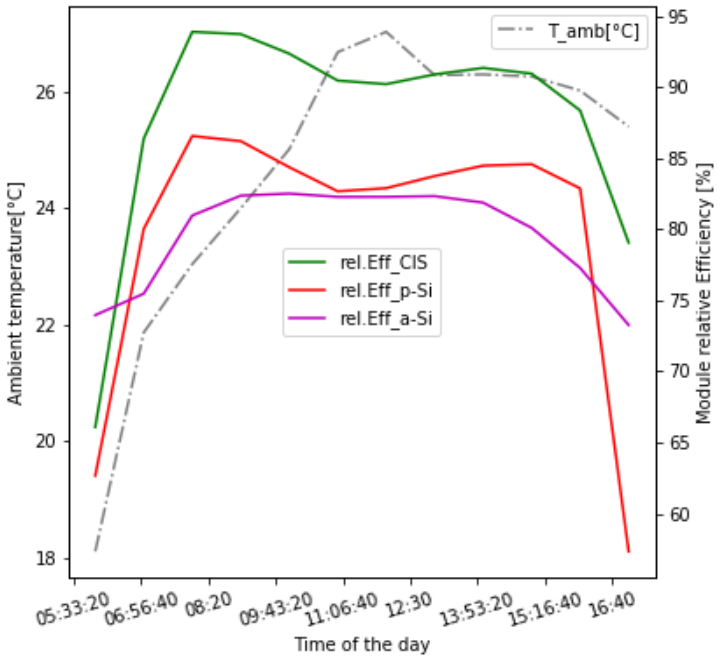

Figure 4.9: Variation in T_{amb} and relative efficiency on the sunny day of 17 December 2015 in PE.

It can be observed from figure 4.9 that, when the ambient temperature is highest, CIS and p-Si modules experience a non-negligible decrease in relative efficiency, while the relative efficiency for a-Si remained unaffected by the high temperature. This indicates that the a-Si maintains an output closest to its nominal output and can maintain a steady energy output despite rising temperature, making it suitable for deployment in regions with hot climate.

The variation in ambient temperature and relative efficiency for the cloudy winter day of 04 June 2015 is shown in figure 4.10.

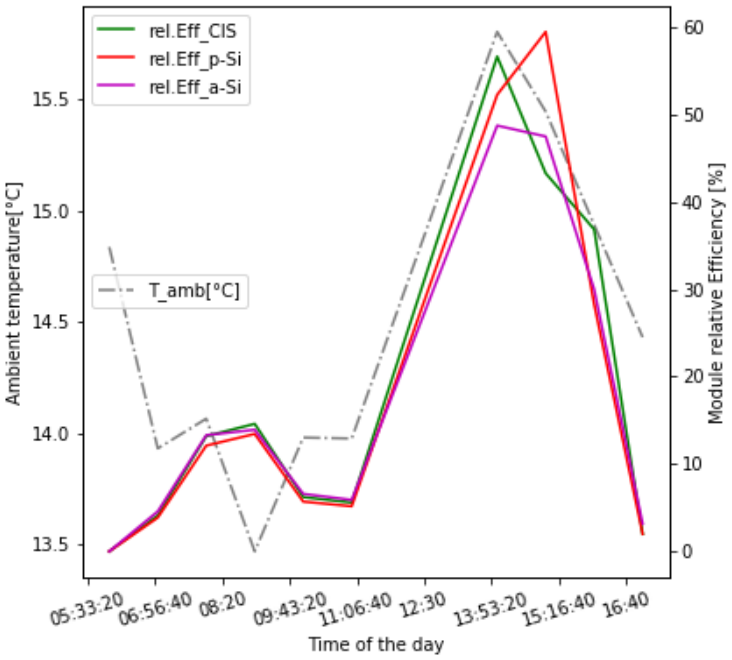

Figure 4.10: Variation in T_{amb} and relative efficiency on the cloudy day of 04 June 2015 in PE.

On the cloudy day, figure 4.10, the mean ambient temperature is well below 20°C, thus the relative efficiency can be observed to be increasing with increasing ambient temperature although the relative efficiency remains relatively low (less than 60%) for all the three modules. On the other hand, it can be observed from figure 4.10 between 8:20 and 9:40 that, the relative efficiency increased when the ambient temperature decreased from 14.0°C to 13.5°C and then decreased when the ambient temperature increased from 13.5°C to 14.0°C. Justification for the observed trend could not be established.

The variation in the relative efficiencies of the three modules for all sunny days is shown in the box plot in figure 4.11. The mean relative efficiencies on sunny days were found to be 92± 3% for CIS, 85± 2% for p-Si and 83± 2% for a-Si. The ANOVA test on the relative efficiencies indicate that the mean relative efficiencies differ among the three module technologies on sunny days ($p = 2.736 \times 10^{-62}$). The post-hoc test showed that at 5 % significant level, the mean daily relative efficiency of each type of module is statistically different from

the mean relative efficiency of every other type of module(p <0.05) on the sunny days. Therefore, on sunny days the average operational efficiency of CIS is 92% of its STC efficiency, while the average operational efficiency of p-Si is 85% of its STC efficiency and the average operational efficiency of a-Si is 83% of its STC efficiency.

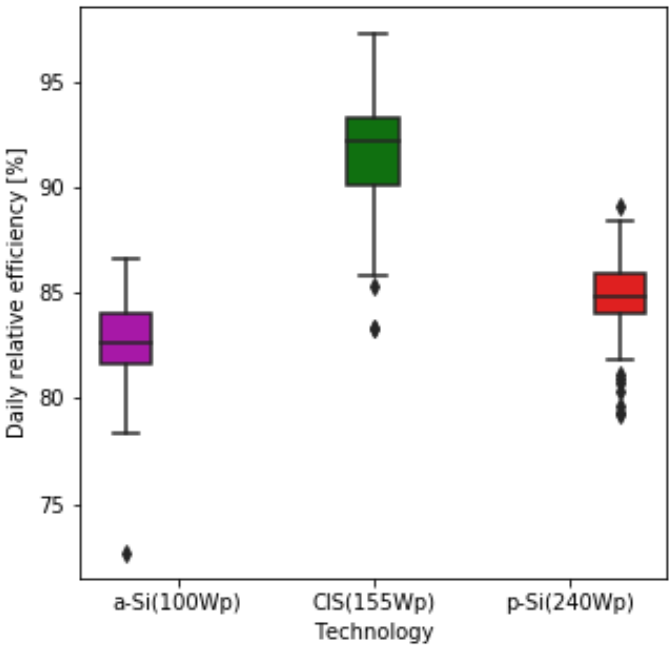

Figure 4.11: Daily module's relative efficiencies for the sunny days in PE.

The variation in the relative efficiencies of the three modules for all cloudy days is shown in the box plot in figure 4.12. On cloudy days, the mean relative were found to be 87± 14% for CIS, 86± 12% for a-Si and 85± 12% for p-Si. The ANOVA test on the relative efficiencies indicate that there is no statistical difference on cloudy days (p <0.05). Therefore, in the cloudy conditions, the average efficiency of a module is approximately 85% of its respective STC efficiency for any of the three technologies, which means that in cloudy conditions the average operational efficiency of p-Si will be highest.

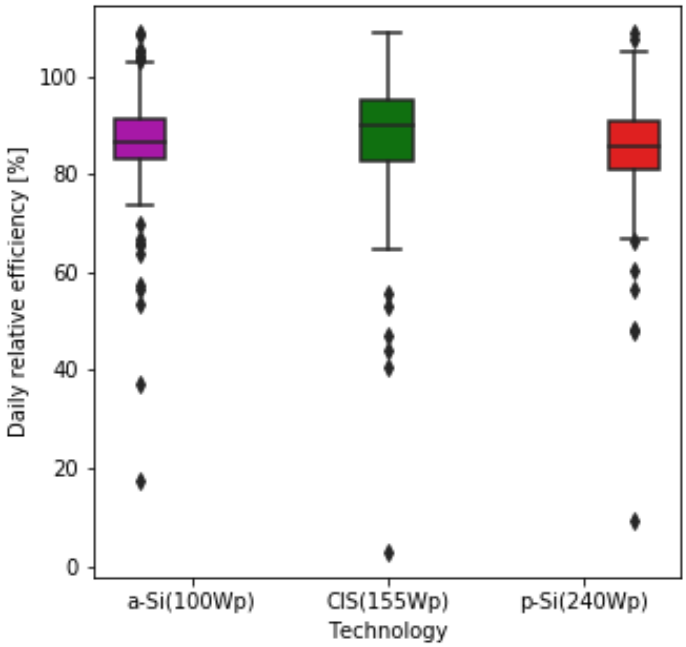

Figure 4.12: Daily module's relative efficiencies for the cloudy days in PE.

Under the deployment conditions of PE, CIS reached the highest mean relative efficiency, followed by p-Si and a-Si yielded the lowest during the sunny days. The results obtained by [31] [9] [11] [10] showed that the performance of p-Si modules is strongly influenced by module temperature, while the contribution of solar spectrum is quite minimal while the power output of a-Si PV module mainly depends on the spectrum distribution with minimal dependence on temperature due to the small temperature coefficient for maximum power.

4.1.4 Specific yield (SY) at PE

The specific yield (SY) was calculated from equation (2.7) in section 2.4.2. The variation in the SY for a single sunny summer day is shown in figure 4.13. The daily mean specific yield for all sunny days is shown in figure 4.14. The mean daily specific yields for the sunny days were found to be
6.52± 0.59kWh/kW$_p$, 5.97 ± 0.55kWh/kW$_p$ and 5.86 ± 0.49kWh/kW$_p$ for CIS, p-Si and a-Si respectively. It can be seen from figure 4.14, that on average for

the sunny days, CIS has the highest daily specific yield compared to the p-Si and a-Si modules.

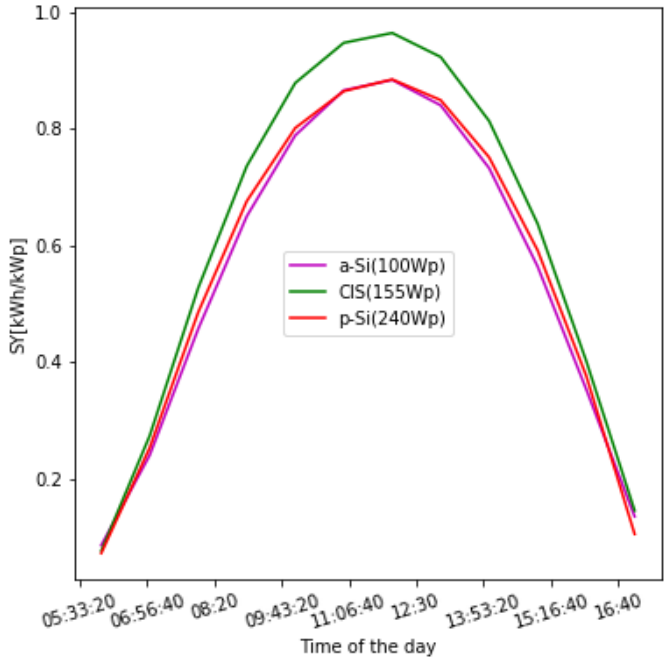

Figure 4.13: Variation in specific yield as a function of time of the day for the sunny day of 17 December 2015 in PE

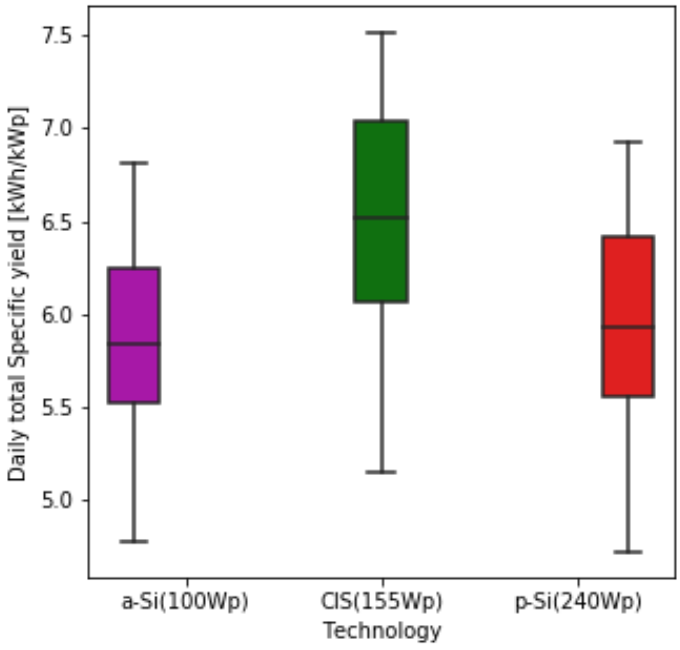

Figure 4.14: Daily total specific yields for the sunny days in PE.

The ANOVA test on the SY yielded a statistically significant difference in the mean daily specific yield between the modules ($p =< 0.05$) during the sunny days. The post-hoc test showed that, on sunny days, the mean specific yield of the CIS module differs from the others being higher than the mean specific yields of the other two module types. Based on the SY results, CIS produced about 9% more energy per installed power than both p-Si and a-Si modules.

The daily mean specific yield for all cloudy days is shown in figure 4.15. The mean daily specific yields for the cloudy days were found to be $1.49\pm 1.65 kWh/kW_p$ for CIS, $1.41\pm 1.50 kWh/kW_p$ for p-Si and $1.43\pm 1.49 kWh/kW_p$ for a-Si. The ANOVA test on the specific yield indicated that there is no statistical difference between the mean specific yields of any modules during cloudy days ($p<0.05$).

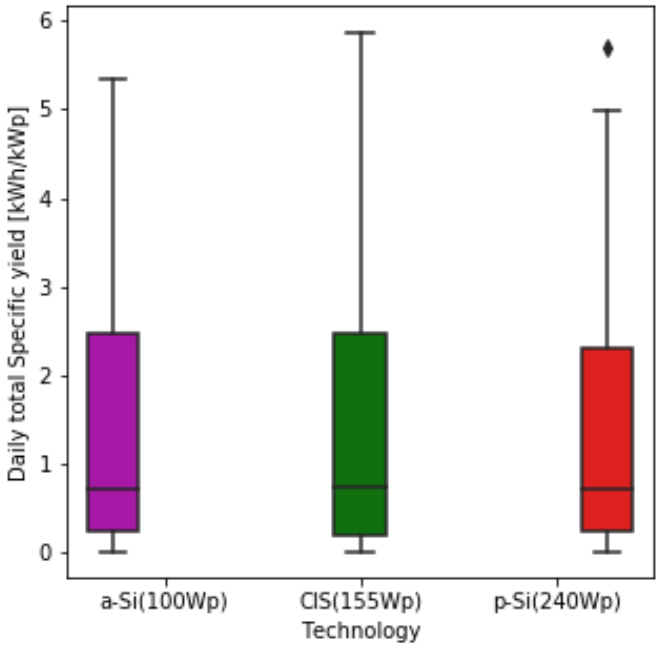

Figure 4.15: Daily total specific yields for the cloudy days in PE.

The sunny days data was further analysed to assess the relationship between the specific yield and ambient conditions, like solar radiation and ambient temperature. The scatter plots in figure 4.16 show a strong positive correlation

between the SY and the solar radiation for all the modules. The SY for CIS shows a strongest correlation with the solar radiation (r = 0.742) while a-Si has the weakest (r = 0.709). This indicates that, variation in solar radiation has the strongest effect on the SY of CIS and the least effect on the SY of a-Si. On the other hand, a strong negative correlation between the SY and the ambient temperature can be observed for all the three module types. The strongest negative correlation of SY on ambient temperature was found for CIS (r = -0.502), followed by p-Si (r = -0.500) and a-Si has recorded the least(r = -0.355).

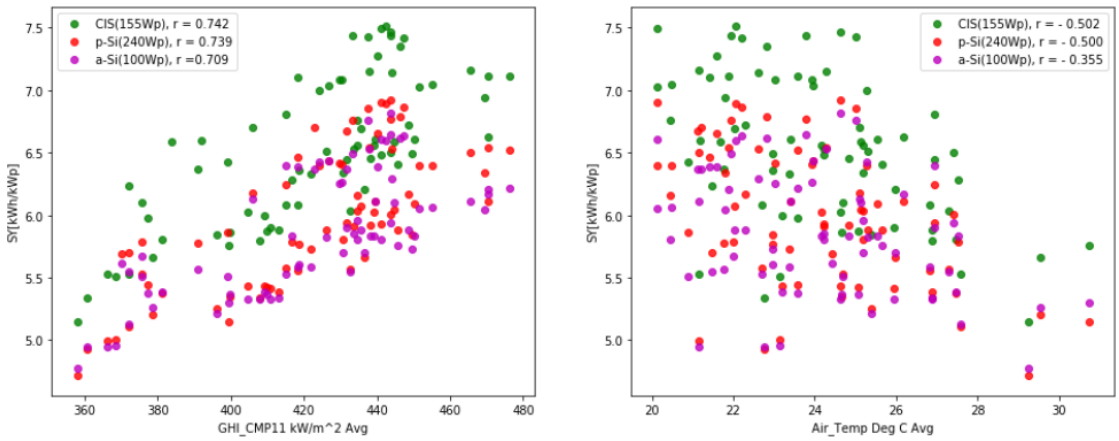

Figure 4.16: Scatter plots showing a strong positive correlation between the SY and GHI (A) but a weaker negative correlation with ambient temperature (B).

A multiple linear regression (MLR) was performed to determine the functional dependence of the SY on the GHI and T_{amb} for the sunny days. The sunny days were considered because the GHI and T_{amb} on sunny days have a consistent temporal variation. It was established that even though the GHI and T_{amb} are correlated, both are significant predictors of the SY. Based on the established correlations between SY and GHI and T_{amb}, the functional dependence of SY on GHI and T_{amb} was considered to be linear and is given by equation (4.1)

$$SY = \mathbf{a}GHI + \mathbf{b}T_{amb} + \mathbf{c}. \tag{4.1}$$

where **a**, **b** and **c** are the regression coefficients.

The regression coefficients represent by how much the mean SY changes when

one independent variable changes by one unit while keeping the other predictor constant. A positive coefficient indicates that, as the value of the independent variable increases, the mean value of the dependent variable also tends to increase and vice-versa for the negative coefficient. The uncertainty in the estimation of the regression coefficient is reported by the 95 % confidence interval (CI).

The 95 % CI is a range of values that one can be 95% certain to contain the true value of the regression coefficient. The narrower the CI, the better the estimate of the regression coefficient. For a significant regression coefficient, the CI should not contain zero. If the CI contains zero, then it means that the regression coefficient can be zero, which makes such coefficient not significant in the regression model. If the CI is wide, then not much is really known about what is the true value of the regression coefficient. Table 4.2 presents the regression coefficients and their confidence intervals (CI). It can be seen from table 4.2 that the SY for CIS increases the most for a unit increase in solar radiation while a-Si experiences the least drop in SY with increasing ambient temperature.

Table 4.2: SY unstandardized linear regression coefficients of equation (4.1).

Technology	**a** [hm^2/kW]	95% CI	**b** [$h\,°C^{-1}$]	95% CI	**c** [h]	95% CI
CIS	0.0136	[0.011, 0.017]	-0.0869	[-0.123, -0.051]	2.8686	[1.196, 4.541]
p-Si	0.0126	[0.010, 0.015]	-0.0787	[-0.113, -0.045]	2.5658	[0.973, 4.158]
a-Si	0.0112	[0.008, 0.014]	-0.0393	[-0.074, -0.005]	2.0720	[0.451, 3.693]

The graphic representation of the regression equation for each module is shown in figure 4.17. It can be seen from figure 4.17 that CIS produces the greatest SY for all irradiance and ambient temperature conditions on sunny days. The p-Si module has greater SY than a-Si at low temperature and high solar radiation. However, at high temperature and low irradiance p-Si suffers greater loss in power and SY than a-Si because p-Si has larger (more negative) power temperature coefficient, thus a drop in SY for p-Si below that of a-Si as observed in figure 4.17.

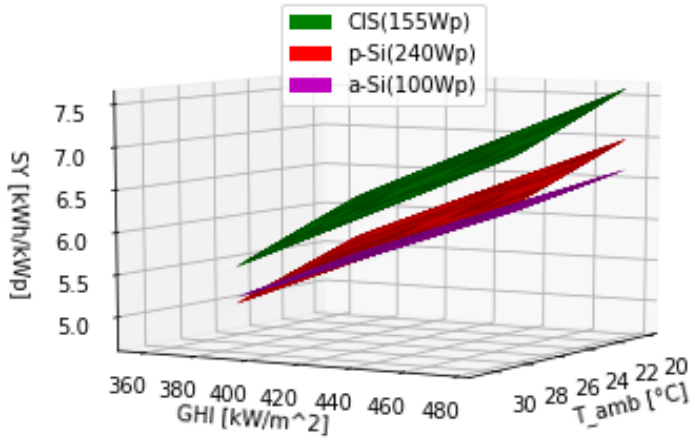

Figure 4.17: Dependence of SY on GHI and T_{amb} for all technologies during the sunny days in PE according to the regression equation (4.1).

Graphs of model's residuals can be used to assess the goodness of the regression model. A residual is the difference between the measured and the fitted value. If the regression model correctly describes the dependence of the dependent variable on the independent variables, the residuals should appear random, without any pattern, on a residuals vs modelled (fitted) value graph. Similarly, if the model is correct, then the residuals should follow a normal probability distribution.

The residuals vs the fitted values of our models are shown in figure figure 4.18 for CIS, figure 4.19 for p-Si and figure 4.20 for a-Si. On the residuals vs the fitted values plots (A graphs), if the points are randomly dispersed around the zero line, the functional form of the linear regression model is appropriate for the data. If the residuals fall on a straight line on the Q-Q plots (B graphs), then they are normally distributed.

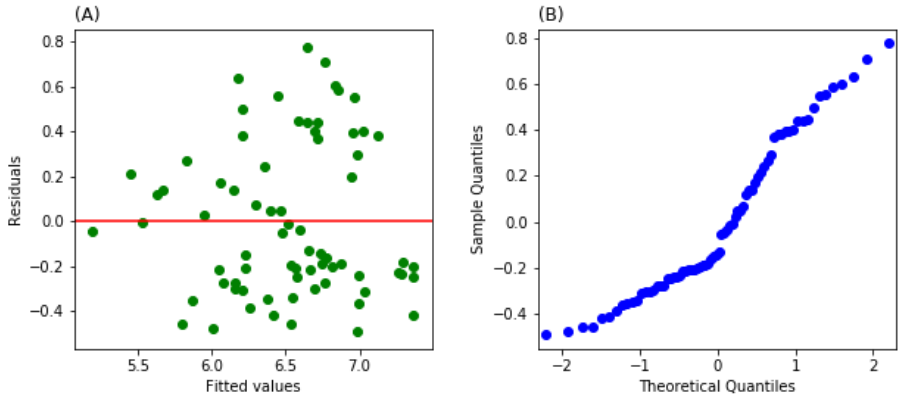

Figure 4.18: SY residuals vs Fitted values (A) and the probability plot (B) for CIS.

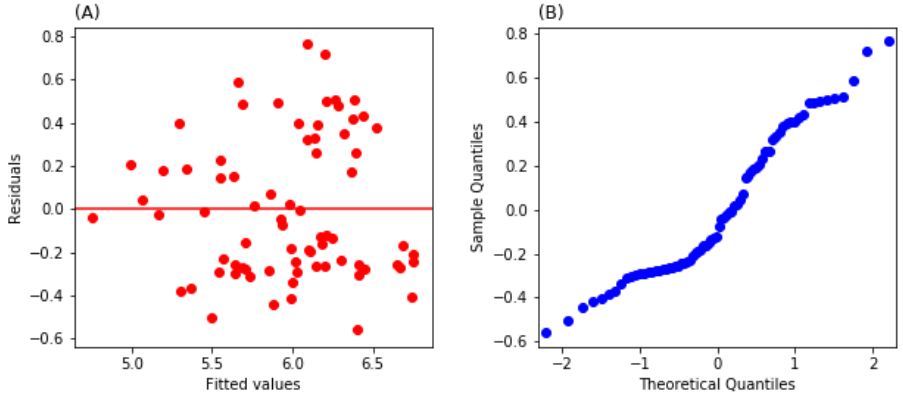

Figure 4.19: SY residuals vs Fitted values (A) and the probability plot (B) for p-Si.

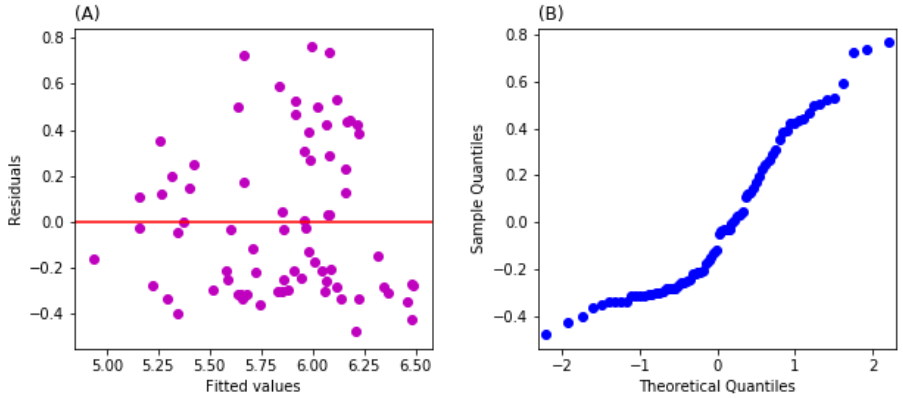

Figure 4.20: SY residuals vs Fitted values (A) and the probability plot (B) for a-Si.

From the plot of residuals vs the fitted values plots figure 4.18(A) for CIS, figure 4.19(A) for p-Si and figure 4.20(A) for a-Si, it can be seen that the residuals

show an increase in variance. The Q-Q plots (B graphs) show that the residuals are not normally distributed. The reasons for the observed non-constant variance and deviation from normal distribution of the residuals could be a missing predictor variable. It appears that an ambient condition like wind speed should be included in the model. Unfortunately, measured wind speed data was not available for the period of this study.

4.1.5 Specific yield per area (SY/A) in PE

The SY/A which indicates the SY per land or roof area occupied by 1kW of modules was calculated using equation (2.8) as defined in section 2.4.3. The mean SY/A during the sunny days were found to be 0.88± 0.08 $\mathrm{kW\,h\,kW_p{}^{-1}\,m^{-2}}$ for p-Si, 0.82± 0.07 $\mathrm{kW\,h\,kW_p{}^{-1}\,m^{-2}}$ for CIS and 0.37± 0.03 $\mathrm{kW\,h\,kW_p{}^{-1}\,m^{-2}}$ for a-Si. The variation in SY/A on sunny days is presented in figure 4.21.

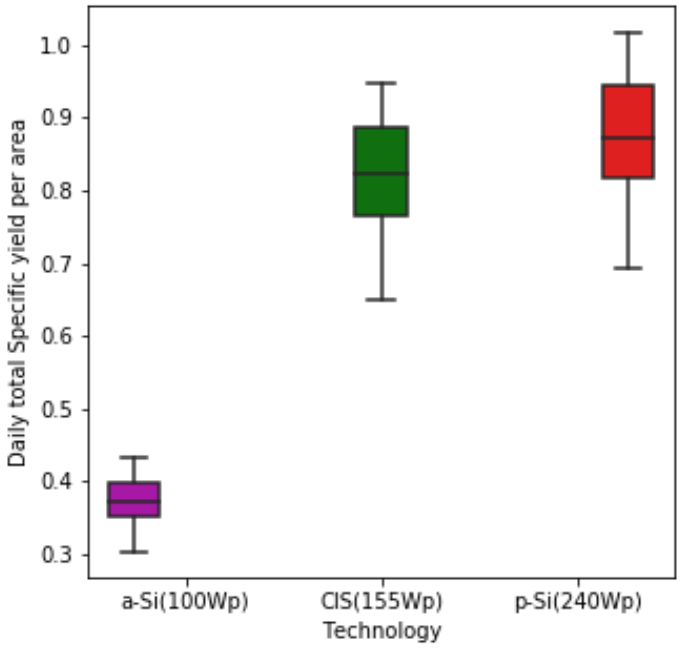

Figure 4.21: Daily total SY/A for the sunny days in PE.

From figure 4.21 it is evident that the specific yield per area, SY/A, of the a-Si modules is significantly smaller than the SY/A of the other two technologies

but the graphical comparison does not allow adequate assessment of potential difference in this performance criterion between p-Si and CIS. The result of the ANOVA test is a very small p-value ($p=1.43 \times 10^{-121}$) which is a clear indication that there is a difference between the mean specific yields per area of all technologies for the sunny days. The post-hoc test during sunny days, showed that statistically significant difference exists between the SY/A for all technologies. It was found that, the module with the highest STC efficiency which is p-Si, produced the highest SY/A while a-Si which has the lowest STC efficiency, produced the least SY/A. Thus the SY/A for p-Si is about 7% more than that of the CIS module and about 58% more than that of the a-Si module under sunny conditions.

The mean SY/A during the cloudy days were found to be $0.21 \pm 0.22 \mathrm{kW\,h\,kW_p{}^{-1}\,m^{-2}}$ for p-Si, $0.19 \pm 0.21 \mathrm{kW\,h\,kW_p{}^{-1}\,m^{-2}}$ for CIS and $0.09 \pm 0.10 \mathrm{kW\,h\,kW_p{}^{-1}\,m^{-2}}$ for a-Si. The variation in SY/A during the cloudy days is presented in figure 4.22.

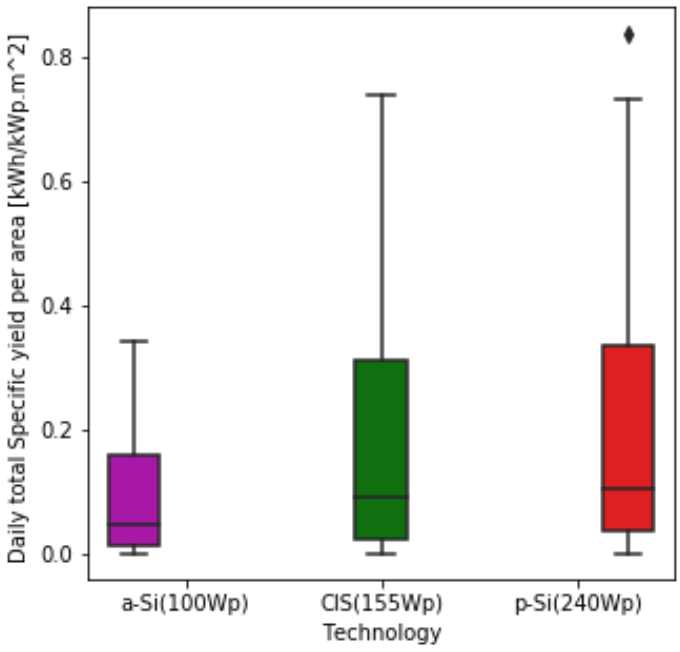

Figure 4.22: Daily total SY/A for the cloudy days in PE.

On cloudy days, the ANOVA test on the SY/A yielded also a statistically

significant difference in the mean daily SY/A between the modules. The post-hoc test showed that only the SY/A for a-Si is different from the others and is lower than that of CIS and p-Si modules, producing 55% less energy per installed 1 kW of area occupied by the modules then that produced by the CIS and p-Si modules.

It can be concluded that, in order to maximize the energy output of the modules when limited installation area is available, the module with the highest efficiency should be used, because it will results in maximum energy output for that given area. The performance results are summarized in table 4.3 at the end of this chapter.

4.2 Assessment at Rosherville, Johannesburg (JHB)

4.2.1 Solar radiation in JHB

The results for JHB are based on the modules temperature and POA irradiance data because GHI and ambient temperature data were not available. The available data for the JHB location is for the period of June to December 2017. According to the Köppen-Geiger climate classication, JHB is classified as sunny, dry and warm. The variation in daily total POA irradiance for each month is shown in figure 4.23.

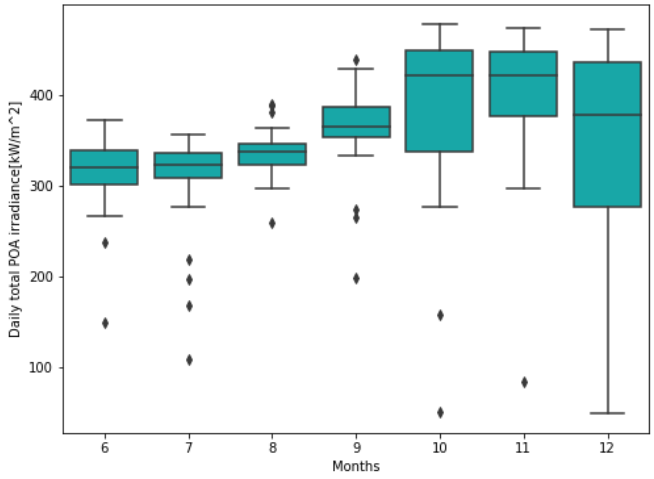

Figure 4.23: Monthly total of daily POA irradiance in JHB.

It can be observed from figure 4.23 that there is much greater variability in the daily total POA irradiance during the months of October to December. The months of July to October shows a small variability in POA irradiance values, indicating the presence of more sunny days during these months.

4.2.2 Module temperatures in JHB

Based on the criteria used to split the data into sunny and cloudy days at the JHB location as described in chapter 3, winter days with daily total irradiance greater than 291.74 $\mathrm{kW\,h\,m^{-2}}$, spring days with daily total irradiance greater than 358.55 $\mathrm{kW\,h\,m^{-2}}$ and summer days with daily total irradiance greater than 354.35 $\mathrm{kW\,h\,m^{-2}}$ were considered sunny. Figure 4.24 shows the variation in total hourly POA irradiance and mean modules temperature as a function of the time of the day on the sunny day of 20 November 2017 while figure 4.25 shows the variation in total hourly POA irradiance and mean modules temperature on the cloudy day of 07 July 2017 in JHB

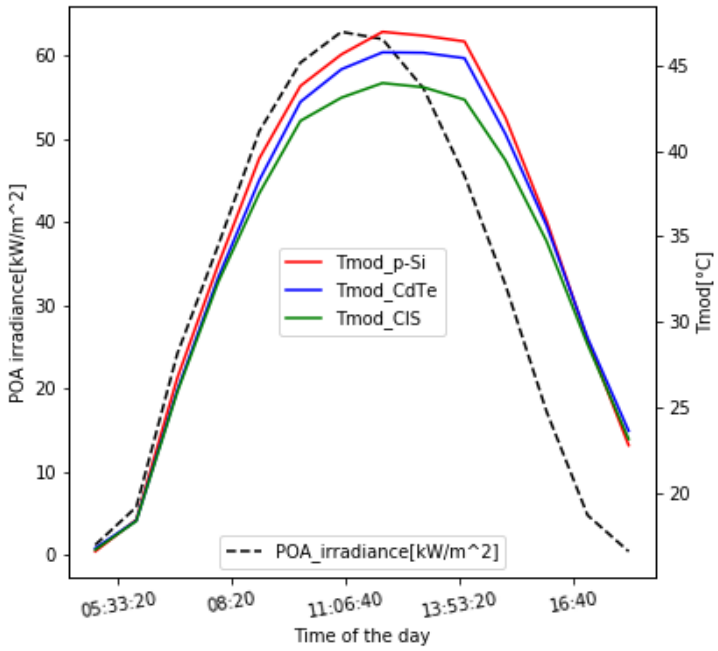

Figure 4.24: Variation in total hourly POA irradiance and mean modules temperature on the sunny day of 20 November 2017 in JHB

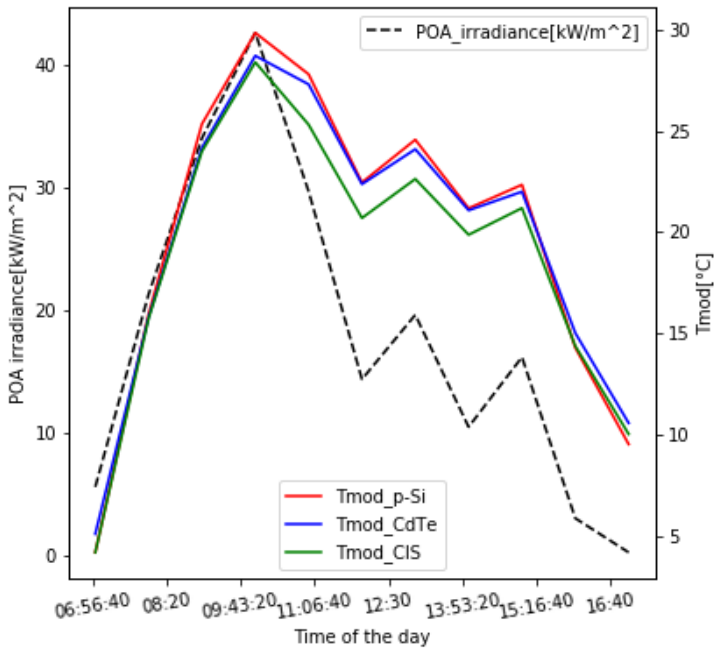

Figure 4.25: Variation in total hourly POA irradiance and mean modules temperature on the cloudy day of 07 July 2017 in JHB.

It can be observed from figure 4.24 and figure 4.25 that p-Si module heated up

the most while CIS remained the coolest. The observed variation in temperatures between the modules is small, in the range of about 3 °C for both sunny and cloudy days, however, this information is vital in predicting which module type will heat up the most on average.

Figure 4.26 gives an overview of the daily mean modules temperature during the sunny days considered in JHB. The daily mean modules temperature on the sunny days were found to be 33.4 ± 2.8°C for p-Si, 32.7 ± 2.9°C for CdTe and 32.1 ± 2.9°C for CIS. The mean modules temperature during the cloudy days is presented in figure 4.27.

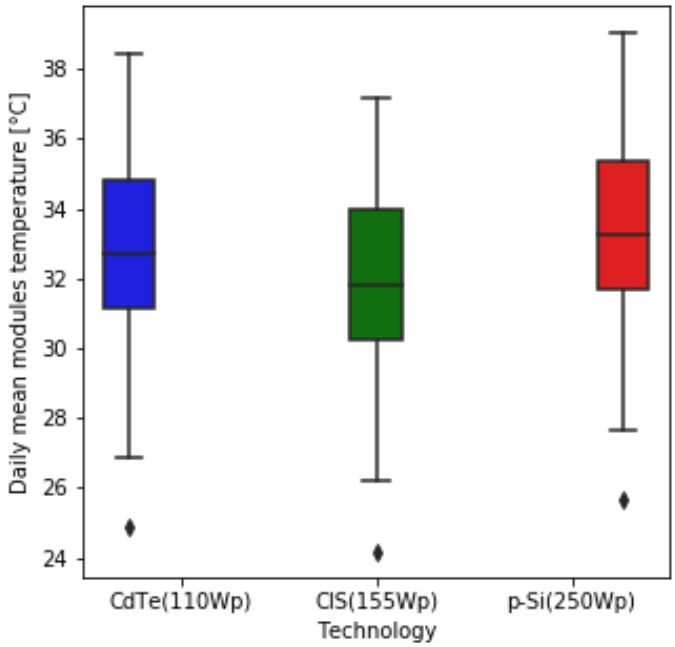

Figure 4.26: Daily mean modules temperature during the sunny days in JHB.

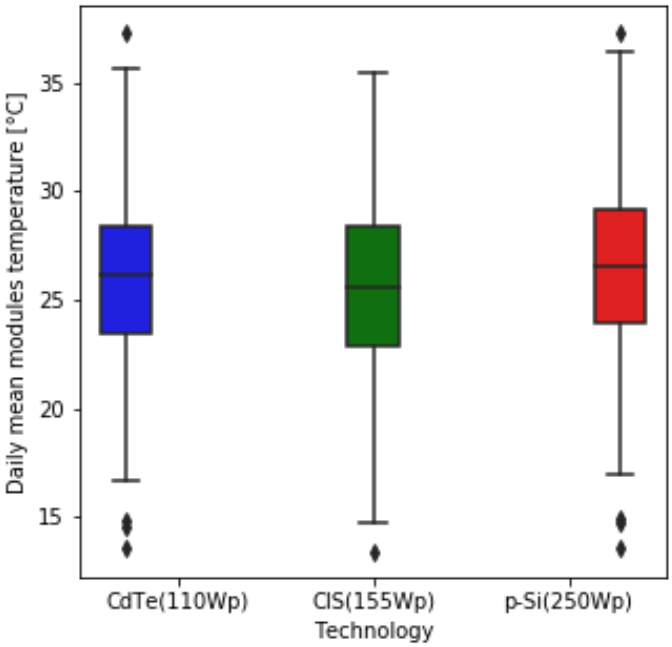

Figure 4.27: Daily mean modules temperature during the cloudy days in JHB.

Based on observations from figure 4.26 and figure 4.27 alone, it is difficult to determine whether a difference exists or not between the mean modules temperature on sunny and cloudy days. However, the ANOVA test on the modules temperature has indicated that there is a statistically significant difference between the daily mean modules' temperature between the technologies ($p = 0.013$) during the sunny days and none exist during the cloudy days . The post-hoc test indicates that only the mean module temperature of p-Si and CIS are statistically different from each other while the mean module temperatures of CdTe is not significantly different from that of p-Si or of CIS on the sunny days in JHB. The p-Si module remained the hottest on average during the sunny days.

4.2.3 Relative efficiency ($\eta_{rel.}$) in JHB

The relative efficiencies were calculated with equation (2.6) in chapter 2. The variation in POA irradiance and relative efficiencies of the modules on the sunny day of 20 November 2017 and cloudy day of 07 July 2017 is shown in figure 4.28

and figure 4.29,respectively.

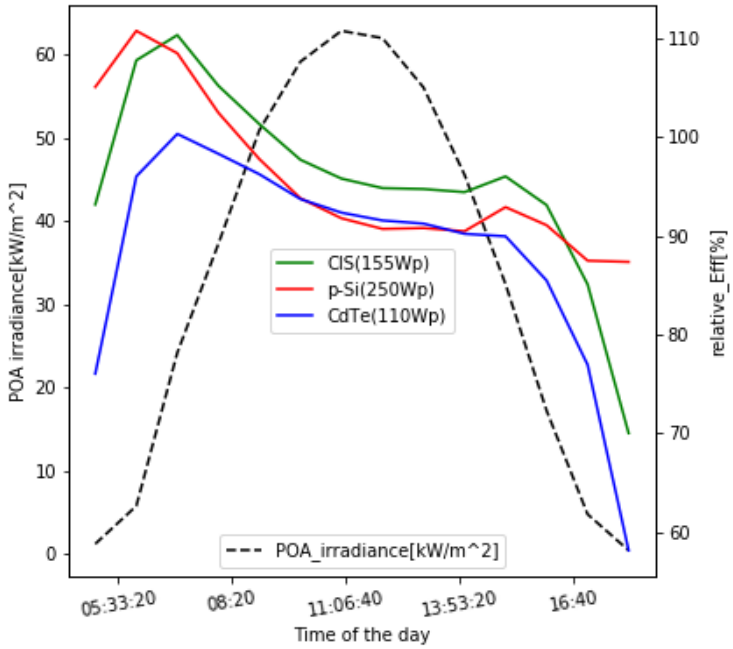

Figure 4.28: Variation in total hourly POA irradiance and mean modules relative efficiency on the sunny day of 20 November 2017 in JHB.

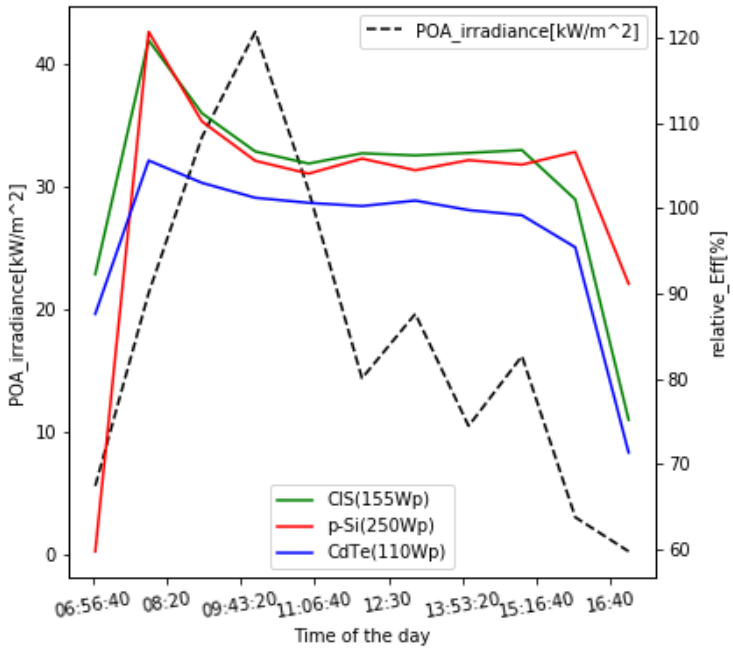

Figure 4.29: Variation in total hourly POA irradiance and mean modules relative efficiency on the cloudy day of 07 July 2017 in JHB.

Analysing figure 4.28 in relation to Figure 4.24 for the single sunny day, it can be concluded that, during the morning hours the modules are cool, the increase in solar radiation results in the increase in relative efficiency. Around noon, when both the POA and modules temperatures are maximum (as observed from Figure 4.24), the relative efficiency decreases and only increase slightly after noon as modules starts cooling down. It can also be observed from figure 4.28 that the p-Si module experienced the greatest decrease in relative efficiency around noon and a-Si module experienced the least. This is attributed to the fact that the p-Si has the largest temperature coefficient(most negative) for maximum power and CdTe has the smallest temperature coefficient. This means, the p-Si module suffers the greatest loss in maximum power for module temperatures above the 25 °C STC temperature compared to CIS and CdTe modules.

During the cloudy day, all modules maintained nearly constant relative efficiencies around noon when the modules temperatures were below 25°C as observed from figure 4.29 and figure 4.25.

For the sunny days, the daily mean relative efficiencies were found to be 97 % for p-Si, 96 % for CIS and 89 % for CdTe. During the cloudy days, the daily mean relative efficiencies were found to be 99 % for p-Si, 97 % for CIS and 90% for CdTe. The variation in daily mean relative efficiencies for the sunny days and the cloudy days are shown in figure 4.30 and figure 4.31, respectively.

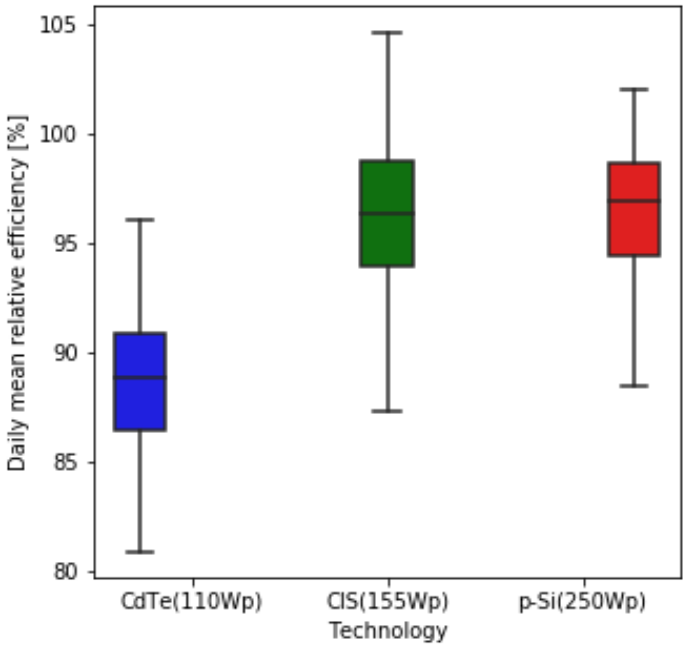

Figure 4.30: Daily mean modules relative efficiency on the sunny days in JHB.

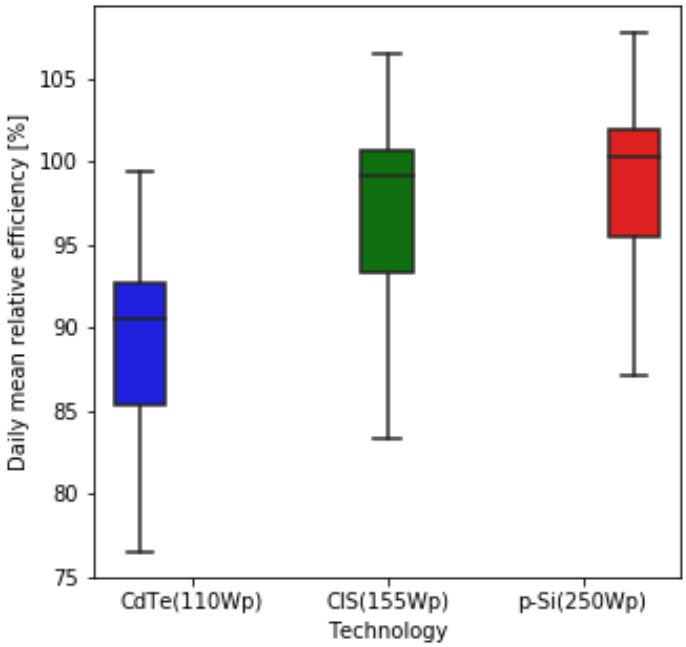

Figure 4.31: Daily mean modules' relative efficiency on the cloudy days in JHB.

The ANOVA test on the relative efficiency indicates that there is a statistically significant difference between the mean relative efficiencies of the modules for

both sunny and cloudy days. The post-hoc test showed that, on both sunny and cloudy days, only the mean relative efficiency for CdTe is statistically different from that of the other two technologies, with CdTe having the smallest mean relative efficiency. No significant difference exists between p-Si and CIS. The relative efficiency of the CdTe module averages nearly 10 % below the relative efficiencies of p-Si and CIS on both sunny and cloudy days. It is interesting to note that the p-Si and CIS modules retain high relative efficiencies during the cloudy days at this location. The low relative efficiency for CdTe might be due to the module's higher series resistance which leads to higher power losses in high irradiance conditions.

4.2.4 Specific yield (SY) in JHB

The specific yields were calculated from equation (2.7). The variation in daily total specific yield for the sunny days and cloudy days is presented in figure 4.32 and figure 4.33, respectively. The daily total specific yields for the modules on the sunny days were found to be 6.92± 0.57kWh/kW_p for CIS, 6.55± 0.55kWh/kW_p for CdTe and 6.43 ± 0.53kWh/kW_p for p-Si.

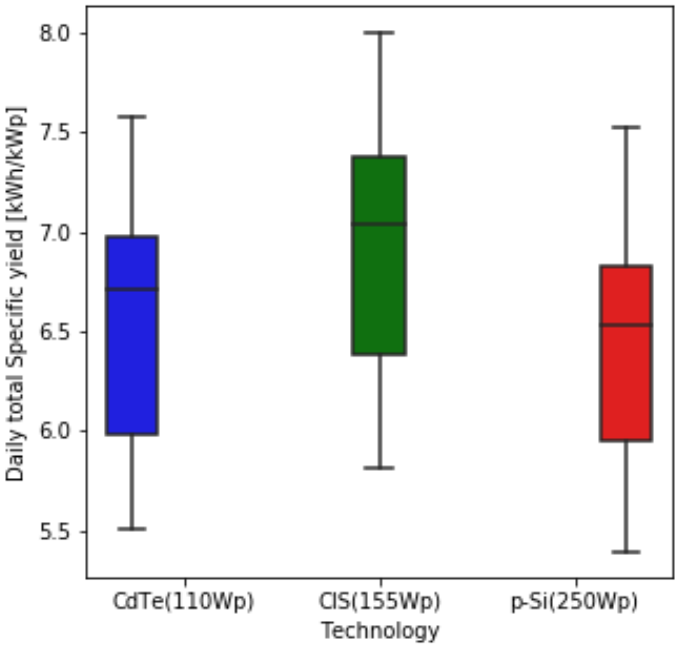

Figure 4.32: Daily total specific yields on the sunny days in JHB.

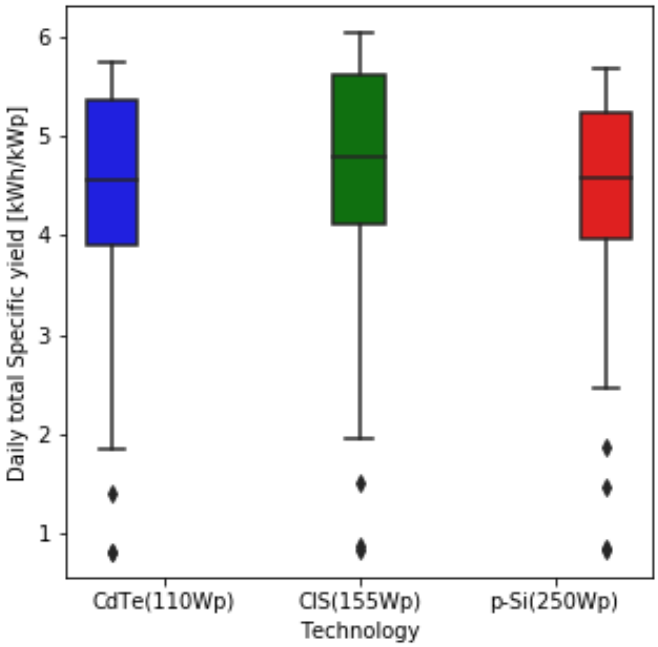

Figure 4.33: Daily total specific yields on the cloudy days in JHB.

The ANOVA test on the daily total SY indicated a statistically significant difference in mean specific yields between the technologies ($p = 1.394 \times 10^{-7}$)

for the sunny days while no difference exist for the cloudy days. The post-hoc test indicates that on the sunny days, only the mean specific yield for CIS is statistically different from that of the other two technologies. This means that, on cloudy days all modules perform similarly in terms of SY and only on sunny days the CIS out performs the others, producing about 6% more SY than the CdTe and p-Si modules.

4.2.5 Specific yield per area (SY/A) in JHB

The SY/A was calculated from equation (2.8). The daily total SY/A for the PV technologies at the JHB location during the sunny days is shown in figure 4.34 and 4.35.

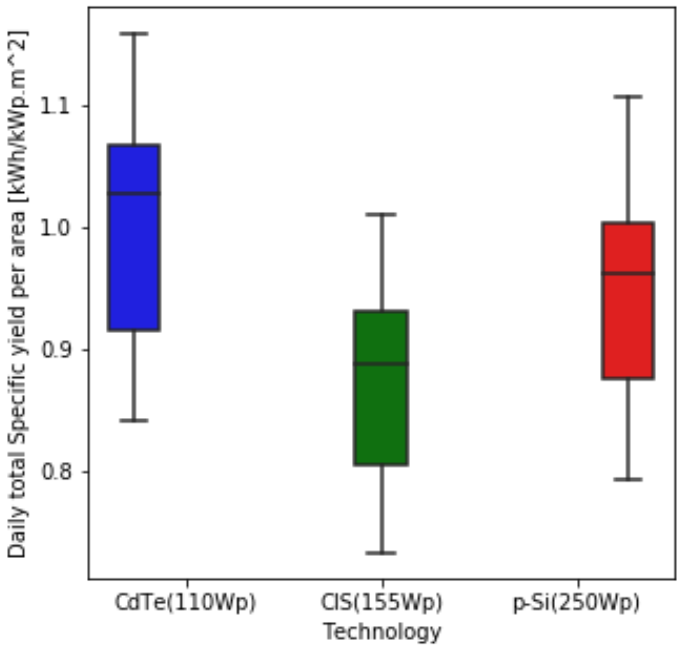

Figure 4.34: Daily total SY/A on the sunny days in JHB.

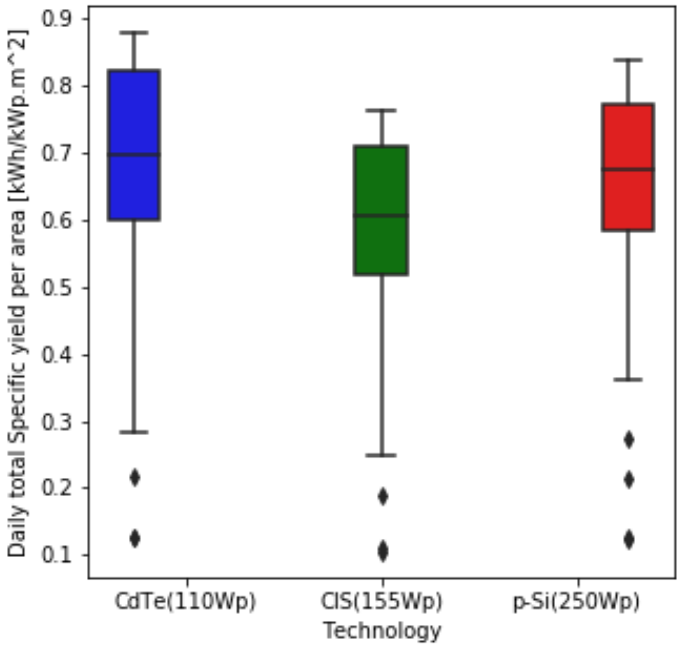

Figure 4.35: Daily total SY/A on the cloudy days in JHB.

The ANOVA test on the SY/A yielded a statistically significant difference in mean SY/A between the technologies ($p = 1.199 \times 10^{-20}$) on both sunny and cloudy days. The post-hoc test indicated that the mean SY/A for all technologies are statistically different from each other on sunny days. CdTe yielded the highest SY/A of 1.00± 0.08kW h $kW_p{}^{-1}$ m^{-2}, followed by p-Si with SY/A of 0.95 ± 0.08kW h $kW_p{}^{-1}$ m^{-2} and CIS with SY/A of 0.87 ± 0.07kW h $kW_p{}^{-1}$ m^{-2}. This means, under sunny conditions, the SY/A for a CdTe module will about 5% more than that of a p-Si module and about 13% more than that of a CIS module.

During the cloudy days, the difference in SY/A only exist between CdTe and CIS. The mean daily SY/A on cloudy days were found to be 0.66± 0.19kW h $kW_p{}^{-1}$ m^{-2} for CdTe, followed by p-Si with SY/A of 0.63 ± 0.18kW h $kW_p{}^{-1}$ m^{-2} and CIS with SY/A 0.57 ± 0.17kW h $kW_p{}^{-1}$ m^{-2}. This means,under cloudy conditions, the SY/A for a CdTe module is about 14% more than that of a p-Si and CIS module. Therefore, in the JHB location, if the space is limited, installing the CdTe modules will yield the maximum output out of that area on both sunny

and cloudy days.

4.3 Chapter 4 Summary

This chapter presented the performance of different types of PV technologies in relation to the deployment climate. Table 4.3 summarises the results from both locations, PE and JHB. The modules are ranked from the one with the highest performance (in bold) to the one with the least performance. When more than one modules are in bold, that indicates that they are equally ranked, based on the statistical results.

Table 4.3: Summary of performance results at both locations

Performance indicator	PE Sunny days	PE Cloudy days	JHB Sunny days	JHB Cloudy days
SY	**CIS**, p-Si, a-Si	Same performace	**CIS**, CdTe, p-Si	Same performance
SY/A	**p-Si, CIS**, a-Si	**p-Si, CIS**, a-Si	**CdTe**, p-Si, CIS	**CdTe**, p-Si, CIS
η_{rel}	**CIS, p-Si**, a-Si	Same performance	**p-Si, CIS**, CdTe	**p-Si, CIS**, CdTe
T_{mod}[b]	Same performance	Same performance	**p-Si**, CdTe, CIS	Same performance

[b]Not a performance indicator. The module in bold is the hottest.

Chapter 5

Conclusion and Recommendations

5.1 Introduction

This chapter presents the conclusions drawn from our results and offers some recommendations for the choice of the most suitable module types under different conditions, the limitations and areas of further research ends the chapter.

The purpose of this research was to collect climate data and energy output of different types of PV technologies deployed at two different climatic conditions and determine whether there might be compelling reasons for the preference of a specific PV technology for deployment in particular climatic conditions.

5.2 Summary of the research

Measurements were taken at two stations in South Africa with different climates: Port Elizabeth (PE), having a warm semi-arid climate, and Johannesburg (JHB), having a humid subtropical climate. At PE, one minute interval power output and module temperature were measured from the research station while the GHI and ambient temperatures were obtained from the SAURAN website, this data is for a period of 1 year. One minute interval power output of the modules and

irradiance incident on the modules were measured for JHB during a period of 6 months.

The performance assessments were based on the following performance indicators: specific yield (SY), specific yield per unit land/roof area occupied by modules (SY/A) and the relative module efficiency ($\eta_{rel.}$) for sunny days and cloudy days in each location.

ANOVA statistical test and Tukey post-hoc test at 5% significance level were used for comparison of the daily SY, SY/A, ($\eta_{rel.}$) and average module temperatures between the different technologies at each location. These tests were chosen because they compare means of at least three or more groups and there were at least three PV technologies at each research location. A regression model was created to determine the extent of the effect of ambient conditions like irradiance and ambient temperature on the SY of the modules at the PE site.

5.3 Discussion of major findings

Our findings indicate that both, the solar radiation and ambient temperature, have a great impact on the modules SY, with the SY for all module types increasing linearly with the solar radiation while decreasing linearly with the ambient temperature during sunny days. On cloudy (low irradiance) days, the SY for all module types increases linearly with both increasing solar radiation and ambient temperature.

It was found that, under sunny conditions (high irradiance), which in PE means daily GHI above 291.74kW m^{-2} while in JHB is GHI above 53.97kW m^{-2}, CIS has the highest SY in both locations, CdTe shows the highest SY/A in JB while p-Si shows the highest SY/A in PE, and a-Si shows the lowest SY, SY/A and ($\eta_{rel.}$) in PE. Under cloudy conditions at both locations, the performance of all types of modules were found to be approximate to each other.

Furthermore, CIS remained the coolest and p-Si the hottest in the JHB location. At PE, the average module temperatures were comparable on both sunny

and cloudy days. The performance of the modules at the two locations are summarized in table 5.1. The modules are ranked from the one with the highest performance (in bold) to the one with the least performance. When more than one modules are in bold, that indicates that they are equally ranked, based on the statistical results.

Table 5.1: Summary of performance results at both locations

Performance indicator	PE Sunny days	PE Cloudy days	JHB Sunny days	JHB Cloudy days
SY	**CIS** p-Si, a-Si	Same performance	**CIS** CdTe, p-Si	Same performance
SY/A	**p-Si, CIS** a-Si	**p-Si, CIS** a-Si	**CdTe** p-Si, CIS	**CdTe** p-Si, CIS
η_{rel}	**CIS, p-Si** a-Si	Same performance	**p-Si, CIS** CdTe	**p-Si, CIS** CdTe

Based on the results obtained from the modules used in this study, a decision tree, figure 5.1, has been developed to guide the selection of modules for optimal performance for locations that are predominantly sunny or predominantly cloudy. A day of a given season was classified as sunny if its total daily GHI is equal to or greater than 75% of the Maximum daily GHI in that season. Otherwise it is classified as cloudy. A location is therefore termed predominantly sunny if more than 50% of the days have a total daily GHI equal to or greater than 75 % of the Maximum daily GHI in that season. The decision tree is strictly based on the climate of the location and the available land or roof space for the modules and does not consider the cost of the modules.

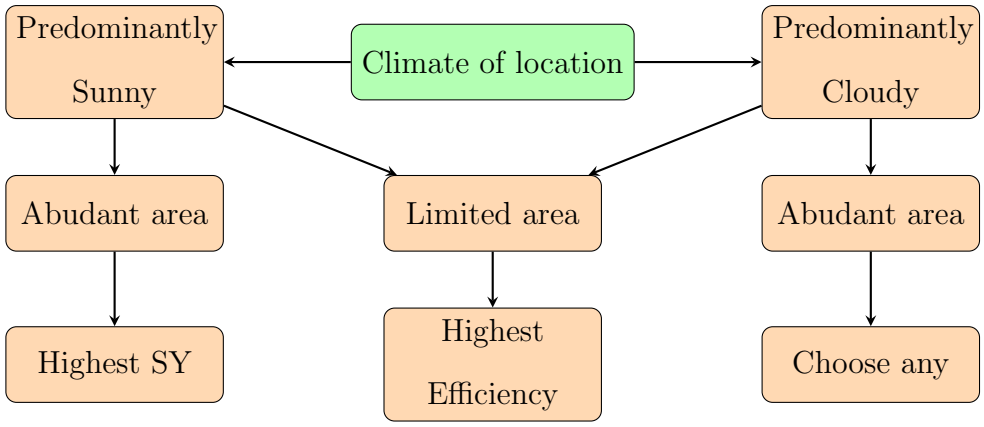

Figure 5.1: Module selection decision tree.

In conclusion, significant difference in performance between technologies is only observed during sunny conditions. The performance cannot be generalised for any PV technologies but depends on the assessed performance indicator. This is because it was found that different PV technologies have shown vast differences in performance between different performance indicators. These results are based only on the first year of module deployment and can be expected to change with time due to module degradation.

5.4 Recommendations

It is recommended that, for sites that are mostly sunny, if the area available for installation is abundant, one should choose the module with the highest SY else if the area is limited, one should choose the module with the highest efficiency. On the other hand, for sites that are mostly cloudy, if the area is limited, one should choose the modules with highest efficiency, else choose any when the installation area is plenty.

5.5 Limitations and areas of further research

Due to a lack of local research facilities in photovoltaics, the energy output of the modules were obtained from the research site at PE. As a result, it was very

difficult to correctly justify why some data were missing and some were very high, resulting in lot of data being cleaned out. In addition, some needed data could not be obtained, for example wind speed, which our analysis indicates has an effect on the SY at both PE and JHB location was not available. Furthermore, the climate data for JHB could not be obtained. This has hindered the performance analysis at that location to be based on the POA irradiance and modules temperature rather than on GHI and ambient temperature. Also, the regression analysis could not be done due to the same reason.

Further research is needed to assess the much reliable long term performance of commercially available PV modules. PV modules are reported to have a lifespan of about 25 years. An assessment on performance and degradation for at least the first 10 years of operation is necessary for reliable choice of suitable PV technology for the greatest return on investment in the modules.

Bibliography

[1] Heinrich Häberlin. *Photovoltaics: system design and practice.* John Wiley & Sons, 2012.

[2] Muriele Bester de Souza, dwin Augusto Tonolo, Renata Lautert Yang, Gerson Mximo Tiepolo, and Jair Urbanetz Junior. "Determination of diffused irradiation from horizontal global irradiation-study for the city of curitiba". 62. Publisher :SciELO Brasil.

[3] M. C. Peel, B. L. Finlayson, and T. A. McMahon. Updated world map of the köppen-geiger climate classification., 12 2007.

[4] Electrical4U. Solar cell: Working principle & construction (diagrams included). Accessed 10 October 2020.

[5] Commons Wikimedia. Kppen-geiger climate classification map.png wikimedia commons, the free media repository. [Online; accessed 3-November-2020].

[6] EMCON. Electricity supply and management options for namibia. a technical and economic evaluation. Accessed 08 March 2017.

[7] SolarGIS. Solargis-africa-and-middle-east-ghi-solar-resource-map-en, 2011.

[8] Ababacar Ndiaye, Cheikh M. F. Kébé, Abdérafi Charki, Papa A. Ndiaye, Vincent Sambou, and Abdessamad Kobi. Degradation of crystalline-silicon photovoltaic modules after a few operation years in a tropical environment. *Solar Energy*, 103:70–77, may 2014.

[9] Tetsuyuki Ishii, Kenji Otani, and Takumi Takashima. Effects of solar spectrum and module temperature on outdoor performance of photovoltaic modules in round-robin measurements in japan. *Progress in Photovoltaics: Research and Applications*, 19:141–148, 2011.

[10] Takashi Minemoto, Yasuhito Nakada, Hiroaki Takahashi, and Hideyuki Takakura. Uniqueness verification of solar spectrum index of average photon energy for evaluating outdoor performance of photovoltaic modules. *Solar Energy*, 83:1294–1299, 2009.

[11] Chattariya Sirisamphanwong and Nipon Ketjoy. Impact of spectral irradiance distribution on the outdoor performance of photovoltaic system under thai climatic conditions. *Renewable energy*, 38:69–74, 2012.

[12] Cristina Cornaro and Angelo Andreotti. Influence of average photon energy index on solar irradiance characteristics and outdoor performance of photovoltaic modules. 21(5):996–1003. Publisher=Wiley Online Library.

[13] Markus Kottek, Jrgen Grieser, Christoph Beck, Bruno Rudolf, and Franz Rubel. World map of the kppen-geiger climate classification updated. *Meteorologische Zeitschrift*, 15:259–263, 7 2006.

[14] C. B. Honsberg and S. G. Bowden. Photovoltaics education website, 2019.

[15] M. Chegaar and P. Mialhe. Effect of atmospheric parameters on the silicon solar cells performance. *Journal of Electron Devices*, 6:173–176, 2008.

[16] P. Wrfel. Solar cell operational principles. *Physics of Solar Cells: From Principles to New Concepts, Wiley-VCH, Weinheim*, pages 1–4, 2005.

[17] Seppo Ovaska. Maximum power point tracking algorithms for photovoltaic applications. Master's thesis, 2010.

[18] Njeru Elosy Gatakaa. 'Performance evaluation of silicon-based photovoltaic modules found in the Kenyan market', 2010.

[19] Martin A. Green. 'Thin-film solar cells: review of materials, technologies and commercial status'. *Journal of Materials Science: Materials in Electronics*, 18:15–19, 2007.

[20] Michael Gostein and Lawrence Dunn. Light soaking effects on photovoltaic modules: Overview and literature review. pages 3126–3131.

[21] K. Wilken, F. Finger, and V. Smirnov. Annealing effects in low temperature amorphous silicon flexible solar cells. 84:17–24. Elsevier.

[22] Solar Frotier. Light soaking effect. Accessed 8 August 2020.

[23] Steven F. Sawyer. Analysis of variance: The fundamental concepts. 17:27–38, 2009.

[24] Thomas Lumley, Paula Diehr, Scott Emerson, and Lu Chen. The importance of the normality assumption in large public health data sets. 23:151–169.

[25] Scott Menard. *Applied logistic regression analysis*, volume 106. Sage.

[26] Glden Kaya Uyank and Nee Gler. A study on multiple linear regression analysis. 106:234–240.

[27] Stephanie Glen. Shapiro-wilk test: What it is and how to run it, 2014.

[28] George Makrides, Bastian Zinsser, Alexander Phinikarides, Markus Schubert, and George E. Georghiou. 'Temperature and thermal annealing effects on different photovoltaic technologies'. *Renewable Energy*, 43:407–417, 2012.

[29] H. D. Mohring and D. Stellbogen. Annual energy harvest of pv systemsadvantages and drawbacks of different pv technologies. pages 1–5, 2008.

[30] E. Ernest Van Dyk, Edson L. Meyer, Bernard J. Scott, Daniel A. O'Connor, and Johan B. Wessels. Analysis of photovoltaic module energy output under operating conditions in south africa. pages 1197–1200, 1997.

[31] G. Nofuentes, J. la Casa, M. Torres-Ramírez, and M. Alonso-Abella. Solar spectral and module temperature influence on the outdoor performance of thin film pv modules deployed on a sunny inland site. *International Journal of Photoenergy*, 2013.

Appendices

Appendix A: Data sheet of the a-Si module

STH SOLAR STH100

TYPICAL PERFORMANCE CHARACTERISTICS	
Typical power (Wp)	100
Tolerance (%)	-0.05
Voltage at max. power (V)	77
Current at max. power (A)	1.29
Open circuit voltage (Voc)	100
Short circuit current (Isc)	1.65

Standard test conditions: 1000W/m2, AM1.5G and 25 degree C

Electrical data above represent stabilized values at Standard test conditions (STC)

MECHANICAL DATA	
Dimension (mm)	L 1414 x W 1110 x T 35
Weight (Kg)	21
Connector	MC or MC equivalent
Cable length (mm)	1000
Cable size (mm2)	2.5

TEMPREATURE COEFFICIENTS	
Maximum power (W)	- 0.20% / C
Maximum power voltage (V)	- 0.32% / C
Maximum power current (A)	+ 0.14% / C
Open circuit voltage (V)	- 0.33% / C
Short circuit current (A)	+ 0.09% / C

INSTALLATION LIMITATIONS	
Maximum system voltage (V)	1000
Operating module temperature	-40C to + 85C
Maximum load	2,4000N/m2 or 245 Kg/m2

CERTIFICATION	
IEC61646	Certified
IEC61730	Certified
UL	Certified

WARRANTY	
Product	12 years
Power output	**Terrestrial:** 12 years / 90% yield

Appendix B: Data sheet of the CdTe module

First Solar

First Solar Series 4™ PV Module

ADVANCED THIN FILM SOLAR TECHNOLOGY

122.5 WATT MODULE
EFFICIENCY OF 17.0%

INDUSTRY BENCHMARK SOLAR MODULES

As a global leader in PV energy, First Solar's advanced thin film solar modules have set the industry benchmark with over 17 gigawatts (GW) installed worldwide and a proven performance advantage over conventional crystalline silicon solar modules. Generating more energy than competing modules with the same power rating, First Solar's Series 4™ and Series 4A™ PV Modules deliver superior performance and reliability to our customers.

PROVEN ENERGY YIELD ADVANTAGE

- Generates more energy than conventional crystalline silicon solar modules with the same power due to superior temperature coefficient and superior spectral response
- Anti-reflective coated glass (Series 4A™) enhances energy production

ADVANCED PERFORMANCE & RELIABILITY

- Compatible with advanced 1500V plant architectures
- Independently certified for reliable performance in high temperature, high humidity, extreme desert and coastal environments
- Visit PlantPredict.com - The only Energy Prediction Software designed for Utility Scale PV

CERTIFICATIONS & TESTS

- PID-Free, Thresher Test, Long-Term Sequential Test, and ATLAS 25+[1]
- IEC 61215/61646 1500V, IEC 61730 1500V, CE
- IEC 61701 Salt Mist Corrosion, IEC 60068-2-68 Dust and Sand Resistance
- ISO 9001:2008 and ISO 14001:2004
- UL 1703 Listed Fire Performance PV Module Type 10[2]
- CSI Eligible, FSEC, MCS, CEC Listed (Australia), SII, InMetro

END-OF-LIFE RECYCLING

- Recycling services available through First Solar's industry-leading recycling program or customer-selected third party.

MODULE WARRANTY[3]

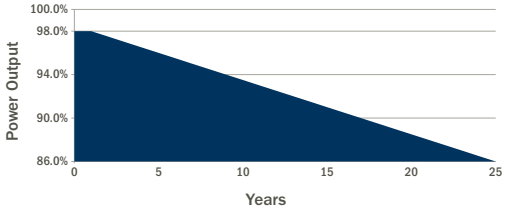

- 25-Year Linear Performance Warranty[4]
- 10-Year Limited Product Warranty

First Solar, Inc. | firstsolar.com | info@firstsolar.com

PD-5-401-04-3 | July 2017

Appendix B: Data sheet of the CdTe module

FIRST SOLAR SERIES 4™ PV MODULE

MECHANICAL DESCRIPTION	
Length	1200mm
Width	600mm
Weight	12kg
Thickness	6.8mm
Area	0.72m²
Individual Leadwire	2.5mm², 657mm (minimum from strain relief to connector mating surface)
Connectors	MC4 or MC4-EVO 2[9]
Bypass Diode	None
Cell Type	Thin-film CdTe semiconductor, up to 216 cells
Frame Material	None
Front Glass	3.2mm heat strengthened Series 4A™ includes anti-reflective coating
Back Glass	3.2mm tempered
Encapsulation	Laminate material with edge seal
Load Rating	2400Pa[10]

MODULE NUMBERS AND RATINGS AT STANDARD TEST CONDITIONS (1000W/m², AM 1.5, 25°C)[5]							
NOMINAL VALUES		FS-4110-3 FS-4110A-3	FS-4112-3 FS-4112A-3	FS-4115-3 FS-4115A-3	FS-4117-3 FS-4117A-3	FS-4120-3 FS-4120A-3	FS-4122-3 FS-4122A-3
Nominal Power[6] (-0/+5W)	P_{MPP} (W)	110.0	112.5	115.0	117.5	120.0	122.5
Voltage at P_{MAX}	V_{MPP} (V)	67.8	68.5	69.3	70.1	70.8	71.5
Current at P_{MAX}	I_{MPP} (A)	1.62	1.64	1.66	1.68	1.70	1.71
Open Circuit Voltage	V_{OC} (V)	86.4	87.0	87.6	88.1	88.7	88.7
Short Circuit Current	I_{SC} (A)	1.82	1.83	1.83	1.83	1.84	1.85
Module Efficiency	%	15.3	15.6	16.0	16.3	16.7	17.0
Maximum System Voltage	V_{SYS} (V)	1500 [7,8]					
Limiting Reverse Current	I_R (A)	4.0					
Maximum Series Fuse	I_{CF} (A)	4.0					
RATINGS AT NOMINAL OPERATING CELL TEMPERATURE OF 45°C (800W/m², 20°C air temperature, AM 1.5, 1m/s wind speed)[5]							
Nominal Power	P_{MPP} (W)	83.2	85.1	87.0	89.0	90.8	92.7
Voltage at P_{MAX}	V_{MPP} (V)	63.5	64.5	64.9	65.9	66.3	67.2
Current at P_{MAX}	I_{MPP} (A)	1.31	1.32	1.34	1.35	1.37	1.38
Open Circuit Voltage	V_{OC} (V)	81.6	82.1	82.7	83.2	83.7	83.7
Short Circuit Current	I_{SC} (A)	1.47	1.47	1.48	1.48	1.48	1.49
TEMPERATURE CHARACTERISTICS							
Module Operating Temperature Range	(°C)	-40 to +85					
Temperature Coefficient of P_{MPP}	T_K (P_{MPP})	-0.28%/°C [Temperature Range: 25°C to 75°C]					
Temperature Coefficient of V_{OC}	T_K (V_{OC})	-0.28%/°C					
Temperature Coefficient of I_{SC}	T_K (I_{SC})	+0.04%/°C					

SUPERIOR SPECTRAL RESPONSE

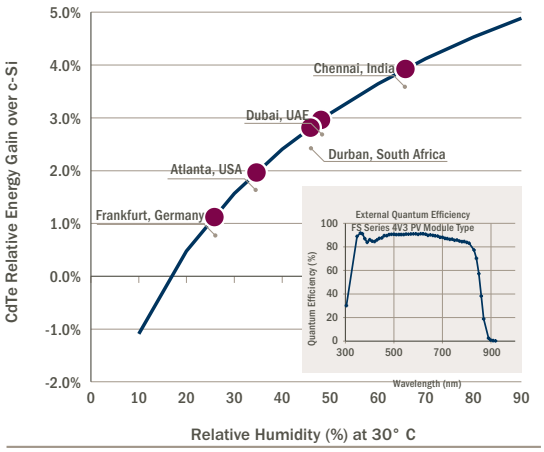

SUPERIOR TEMPERATURE COEFFICIENT

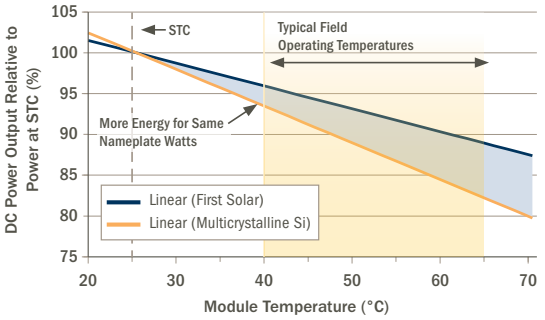

MECHANICAL DRAWING

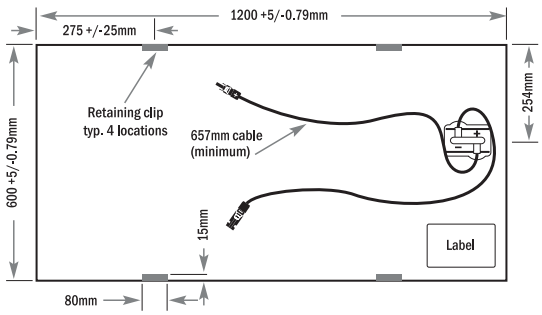

1 Device package meets Atlas 25+
2 Class A Spread of Flame / Class B Burning Brand. Roof mounted fire rating is established by assessing rack and solar module as a unit
3 Limited power output and product warranties subject to warranty terms and conditions
4 Ensures 98% rated power in first year, -0.5%/year through year 25
5 All ratings ± 10%, unless specified otherwise. Specifications are subject to change
6 Measurement uncertainty applies
7 UL 1703 1500V Listed / ULC 1703 1000V Listed
8 Application Class A for 1000V (class II), Application Class B for 1500V (class 0) with MC4; Application Class A for 1000V and 1500V (class II) with MC4-EVO 2
9 Multi-Contact: MC4 (PV-KST4/PV-KBT4) or MC4-EVO 2 (PV-KST-EVO 2 / PV-KBT-EVO 2).
10 Higher load ratings can be met with additional clips or wider clips, subject to testing

firstsolar.com | info@firstsolar.com

Appendix C: Data sheet of the CIS module

PowerModules

SOLAR FRONTIER

Product Overview
SF145-W
SF150-W
SF155-W
SF160-W
SF165-W
SF170-W

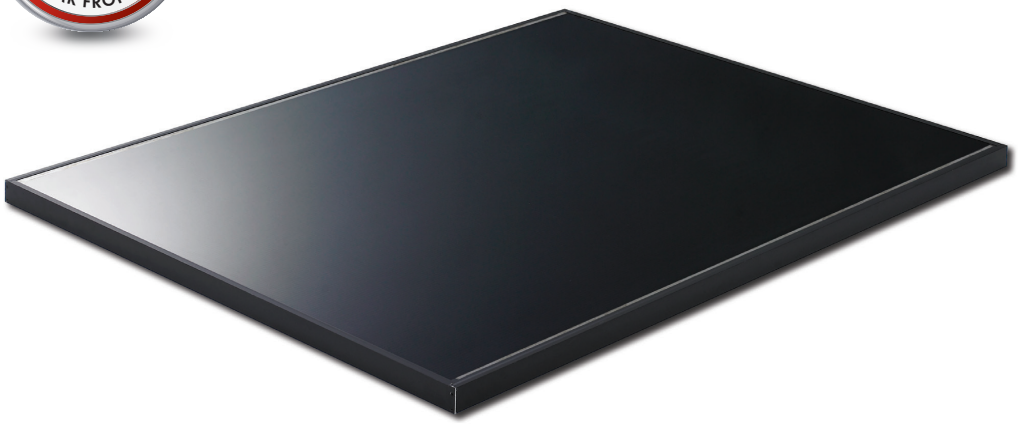

Next Generation CIS

SF145-170-W Modules are certified for static loads up to 5,400 Pa in accordence with IEC 61646. They are therefore suitable for use in snow-rich regions. Solar Frontier's SF145–170 module series offers the highest conversion efficiency of any mass-produced thin-film module, up to 13.8 %. All modules are RoHS compliant and cadmium- and lead-free. Fewer production steps and raw materials also mean an industry-leading energy payback time of less than one year. SF145–170 modules are shipped in cardboard-free packaging and use recyclable corner pieces.

Product & Technology Highlights

- Highest efficiency mass-production thin-film module, up to 13.8 %
- World record 20.9 % achieved in laboratory
- Snow load: 5,400 Pa
- Light Soaking Effect raises output after installation
- Good low-light behavior
- High shadow tolerance
- High temperature stability
- Based on proprietary R&D since 1978
- Cadmium and lead free

www.solar-frontier.eu

Appendix C: Data sheet of the CIS module

SOLAR FRONTIER

I-V Curve

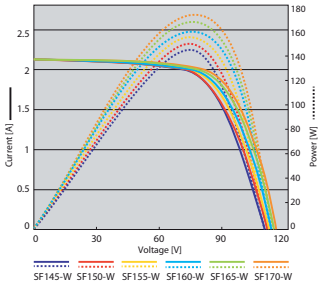

Certificates and Guarantee

All new product classes are subject to immediate certification
Product guarantee: 5 years (extended garantee upon request)
Power output guarantee: 90 % for 10 years, 80 % for 25 years

Module Drawing

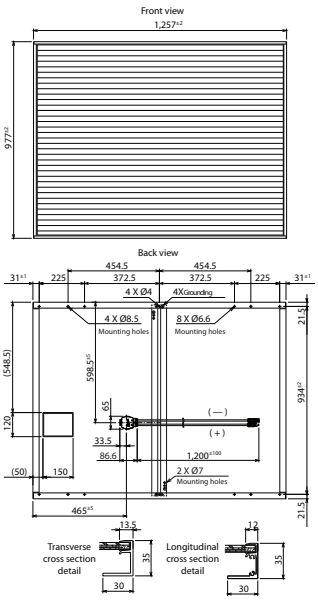

Contact Information

Solar Frontier Europe
Grünwald bei München, Germany
Tel: +49 89 92 86 142 0

Solar Frontier Italy
Bari, Italy | Tel: +39 080 89 66 984

Solar Frontier K.K. (Headquarter)
Tokyo, Japan | Tel: +81 3 5531 5626

Solar Frontier Middle East
Al Khobar, Kingdom of Saudi-Arabia
Tel: +966 3882 0260

Solar Frontier Americas
Santa Clara, CA, USA | Tel: +1 408 916 4150

STC Characteristics

		SF145-W	SF150-W	SF155-W	SF160-W	SF165-W	SF170-W
Nominal power	Pmax	145 W	150 W	155 W	160 W	165 W	170 W
Module efficiency	%	11.8 %	12.2 %	12.6 %	13.0 %	13.4 %	13.8 %
Power tolerance		+5 W/ 0 W					
Open circuit voltage	Voc	107.0 V	108.0 V	109.0 V	110.0 V	110.0 V	112.0 V
Short circuit current	Isc	2.20 A	2.20 A	2.20 A	2.20 A	2.20 A	2.20 A
Voltage at nominal power	Vmpp	81.0 V	81.5 V	82.5 V	84.0 V	85.5 V	87.5 V
Current at nominal power	Impp	1.80 A	1.85 A	1.88 A	1.91 A	1.93 A	1.95 A

Standard Test Conditions (STC): 1,000 W/m² irradiance, module temperature 25 °C, air mass 1.5. Isc and Voc are ±10 % tolerance of STC rated values. Module output may rise due to the Light Soaking Effect. Subject to simulator measurement uncertainty (using best-in-class AAA solar simulator and applying Solar Frontier preconditioning requirements): +10 %/ -5 %.

NOCT Characteristics

		SF145-W	SF150-W	SF155-W	SF160-W	SF165-W	SF170-W
Nominal power	Pmax	108 W	111 W	115 W	119 W	123 W	126 W
Open circuit voltage	Voc	97.4 V	98.3 V	99.2 V	100.0 V	100.0 V	102.0 V
Short circuit current	Isc	1.76 A	1.76 A	1.76 A	1.76 A	1.76 A	1.76 A
Voltage at nominal power	Vmpp	76.0 V	76.4 V	77.4 V	78.8 V	80.2 V	82.1 V
Current at nominal power	Impp	1.43 A	1.47 A	1.49 A	1.51 A	1.53 A	1.55 A

Nominal Operating Cell Temperature Conditions: Module operating temperature at 800 W/m² irradiance, air temperature 20 °C, wind speed 1 m/s and open circuit condition.

Performance at Low Irradiance

Efficiency reduction of maximum power from an irradiance of 1,000 W/m² to 200 W/m² at 25 °C is typically 2.0 %. The standard deviation for the reduction of efficiency is 1.9 %..

Temperature Characteristics

NOCT		47 °C
Temperature coefficient of Isc	α	+0.01 %/K
Temperature coefficient of Voc	β	-0.30 %/K
Temperature coefficient of Pmax	δ	-0.31 %/K

Mechanical Characteristics

Dimensions (L x W x H)	1,257 x 977 x 35 mm (49.5 x 38.5 x 1.4 in.)
Weight	20 kg (44.1 lbs)
Application class (IEC 61730)	Class A
Fire rating (IEC 61730)	Class C
Safety class (IEC 61140)	II
Snow load	5,400 Pa (IEC 61646) / 3,600 Pa design load (UL 1703)
Wind load	2,400 Pa (IEC 61646) / 1,600 Pa design load (UL 1703)
Cell type	CIS glass substrate (cadmium free)
Front cover	Clear tempered glass, 3.2 mm
Encapsulant	EVA
Back sheet	Weatherproof plastic film (color: black & silver)
Frame	Anodized aluminum alloy (color: black)
Edge sealant	Butyl rubber
Junction box	Protection rating: IP67 (with bypass diode)
Adhesive	Silicone
Output cables (conductor)	2.5 mm² / AWG14 (halogen free)
Cable lengths (symmetrical)	1,200 mm (47.2 in.)
Connectors	MC4 compatible
Packing information	25 modules/pallet • 36 pallets/40' container (900 modules)

www.solar-frontier.eu
www.solar-frontier.com

FlyerPowerModules-W-G1-46-PE41

Appendix D: Data sheet of the p-Si module

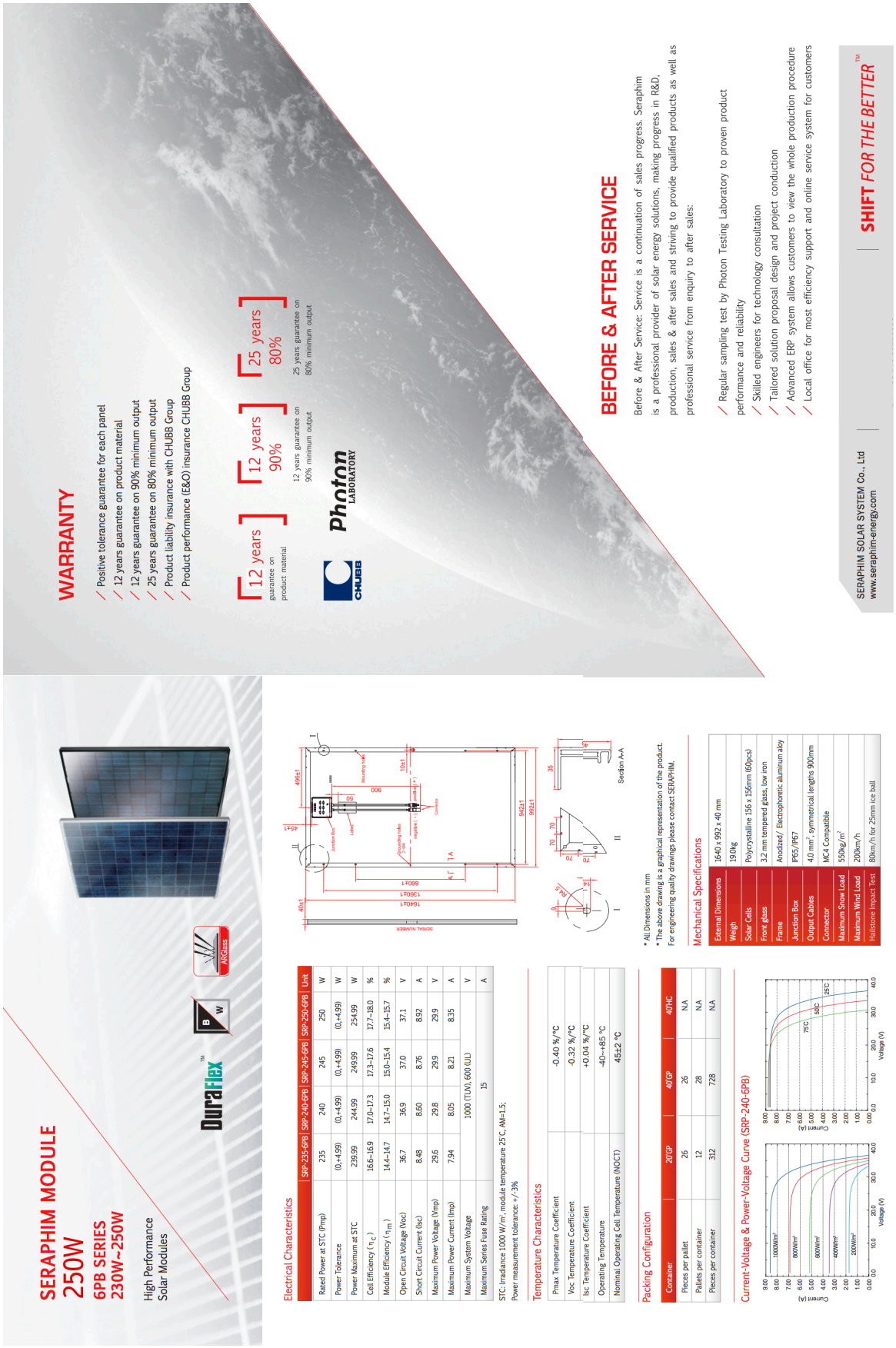

SERAPHIM MODULE
250W
6PB SERIES
230W~250W
High Performance
Solar Modules

DuraFlex™
ARGlass

WARRANTY
- Positive tolerance guarantee for each panel
- 12 years guarantee on product material
- 12 years guarantee on 90% minimum output
- 25 years guarantee on 80% minimum output
- Product liability insurance with CHUBB Group
- Product performance (E&O) insurance CHUBB Group

12 years guarantee on product material
12 years 90% — 12 years guarantee on 90% minimum output
25 years 80% — 25 years guarantee on 80% minimum output
CHUBB
Photon LABORATORY

BEFORE & AFTER SERVICE
Before & After Service: Service is a continuation of sales progress. Seraphim is a professional provider of solar energy solutions, making progress in R&D, production, sales & after sales and striving to provide qualified products as well as professional service from enquiry to after sales:
- Regular sampling test by Photon Testing Laboratory to proven product performance and reliability
- Skilled engineers for technology consultation
- Tailored solution proposal design and project conduction
- Advanced ERP system allows customers to view the whole production procedure
- Local office for most efficiency support and online service system for customers

SERAPHIM SOLAR SYSTEM Co., Ltd
www.seraphim-energy.com
SHIFT FOR THE BETTER™

Electrical Characteristics

	SRP-235-6PB	SRP-240-6PB	SRP-245-6PB	SRP-250-6PB	Unit
Rated Power at STC (Pmp)	235	240	245	250	W
Power Tolerance	(0,+4.99)	(0,+4.99)	(0,+4.99)	(0,+4.99)	W
Power Maximum at STC	239.99	244.99	249.99	254.99	W
Cell Efficiency (η_C)	16.6~16.9	17.0~17.3	17.3~17.6	17.7~18.0	%
Module Efficiency (η_m)	14.4~14.7	14.7~15.0	15.0~15.4	15.4~15.7	%
Open Circuit Voltage (Voc)	36.7	36.9	37.0	37.1	V
Short Circuit Current (Isc)	8.48	8.60	8.76	8.92	A
Maximum Power Voltage (Vmp)	29.6	29.8	29.9	29.9	V
Maximum Power Current (Imp)	7.94	8.05	8.21	8.35	A
Maximum System Voltage	1000 (TUV), 600 (UL)				V
Maximum Series Fuse Rating	15				A

STC: Irradiance 1000 W/m²; module temperature 25°C, AM=1.5;
Power measurement tolerance: +/-3%

Temperature Characteristics

Pmax Temperature Coefficient	-0.40 %/°C
Voc Temperature Coefficient	-0.32 %/°C
Isc Temperature Coefficient	+0.04 %/°C
Operating Temperature	-40~+85 °C
Nominal Operating Cell Temperature (NOCT)	45±2 °C

Packing Configuration

Container	20'GP	40'GP	40'HC
Pieces per pallet	26	26	NA
Pallets per container	12	28	NA
Pieces per container	312	728	NA

Current-Voltage & Power-Voltage Curve (SRP-240-6PB)

* All Dimensions in mm
* The above drawing is a graphical representation of the product. For engineering quality drawings please contact SERAPHIM.

Mechanical Specifications

External Dimensions	1640 x 992 x 40 mm
Weight	19.0kg
Solar Cells	Polycrystalline 156 x 156mm (60pcs)
Front glass	3.2 mm tempered glass, low iron
Frame	Anodized/ Electrophoretic aluminum alloy
Junction Box	IP65/IP67
Output Cables	4.0 mm², symmetrical lengths 900mm
Connector	MC4 Compatible
Maximum Snow Load	550kg/m²
Maximum Wind Load	200km/h
Hailstone Impact Test	80km/h for 25mm ice ball

Appendix D: Data sheet of the p-Si module